

22 **Abstract:** Photosensitivity is observed in numerous autoimmune diseases and drives poor
23 quality of life and disease flares. Elevated epidermal type I interferon (IFN) production primes for
24 photosensitivity and enhanced inflammation, but the substrates that sustain and amplify this
25 cycle remain undefined. Here, we show that IFN-induced Z-DNA binding protein 1 (ZBP1)
26 stabilizes ultraviolet (UV)B-induced cytosolic Z-DNA derived from oxidized mitochondrial DNA.
27 ZBP1 is significantly upregulated in the epidermis of adult and pediatric patients with
28 autoimmune photosensitivity. Strikingly, lupus keratinocytes accumulate extensive cytosolic Z-
29 DNA after UVB, and transfection of keratinocytes with Z-DNA results in stronger IFN production
30 through cGAS-STING activation compared to B-DNA. ZBP1 knockdown abrogates UV-induced
31 IFN responses, whereas overexpression results in a lupus-like phenotype with spontaneous Z-
32 DNA accumulation and IFN production. Our results highlight Z-DNA and ZBP1 as critical
33 mediators for UVB-induced inflammation and uncover how type I IFNs prime for cutaneous
34 inflammation in photosensitivity.

35

36 **One Sentence Summary:** ZBP1 and mitochondrial Z-DNA drive autoimmune photosensitivity
37 via cGAS-STING activation.

38 **Main text:**

39 **INTRODUCTION**

40 Autoimmune photosensitivity is seen in type I Interferon (IFN)-driven skin diseases such as
41 systemic (SLE) and cutaneous lupus erythematosus (CLE) as well as dermatomyositis (DM) (1-
42 4). Up to 81% of SLE and CLE patients are affected by photosensitivity, defined by severe skin
43 reactions to brief ultraviolet light (UV). Photosensitivity leads to poor quality of life for patients(1,
44 5), and in SLE, UV light can also trigger systemic inflammation, including nephritis(1, 6-8).
45 Therapies to prevent photosensitivity are limited to sunscreen use, for which compliance is
46 low(9).

47 The skin is the most common affected organ of lupus patients(10). Nonlesional skin of patients
48 at risk for lupus has been shown to exhibit robust IFN secretion even with minimal IFN signature
49 in the blood(10-12). This cutaneous type I IFN production leads to increased epidermal cell
50 death(3), inflammatory activation of myeloid cells(12), and is widely accepted as a driver of
51 CLE and DM lesions(3, 11, 13, 14). Within the skin, basal keratinocytes (KCs) are the main
52 target of UVB irradiation and are major contributors to the IFN signature observed in these
53 diseases through chronic secretion of IFN kappa (IFN κ)(3, 15, 16). Like type I IFNs, type III IFNs
54 (composed of IFN λ 1-4) are upregulated in CLE skin and may also impact inflammatory
55 responses in photosensitivity(17, 18). It is assumed that the IFN signature in nonlesional skin of
56 lupus patients enhances immune activation and thus contributes to the transition to lesional skin
57 or even systemic disease after environmental triggers, such as UV light(11). However, the
58 precise mechanism by which a cutaneous type I IFN-rich environment accelerates inflammation
59 after UV light has not been identified.

60 The effects of UV light in KCs include mitochondrial DNA damage, mitochondrial fragmentation,
61 and release of mtDNA into the cytoplasm(19-21). UV light is mainly absorbed by complex I of
62 the mitochondrial electron transport chain and leads to reactive oxygen species (ROS)
63 accumulation and disruption of respiratory chain complexes(22). MtDNA is especially
64 susceptible to UV-induced damage as it is not protected by histones, is located in the inner
65 mitochondrial matrix in close proximity to produced ROS, and lacks the same mechanisms that
66 repair nuclear DNA(19). UV light causes type I IFN responses in the skin which is accelerated in
67 autoimmune photosensitivity(1, 2, 23). It has been proposed that this IFN stems from
68 cytoplasmic nucleic acids that activate innate immune sensors. Despite growing evidence that
69 this happens in a cyclic GMP-AMP synthase (cGAS)-stimulator of interferon genes (STING)-

70 dependent fashion(24, 25), the substrate of cGAS activation has not been identified after UV
71 exposure.

72 MtDNA is a major activator of type I IFN responses in multiple autoimmune diseases including
73 SLE(26-30). Specifically, oxidized mtDNA is highly interferogenic in lupus neutrophils(28, 29).
74 Moreover, mtDNA derived from mitochondria-containing red blood cells activates IFN responses
75 in lupus monocytes contributing to the IFN signature observed in SLE blood(31).

76 Mitochondrial dysfunction can lead to liberation of mtDNA into the cytoplasm(27, 32, 33). After
77 release of mtDNA, multiple pattern recognition receptors (PRRs) including Toll-like receptor 9
78 (TLR9), cGAS, and Z-DNA binding protein 1 (ZBP1) can be activated(26, 32-34). ZBP1 itself
79 represents an IFN-induced gene sensing nucleic acids in Z-conformation with its Z α domain to
80 provide antiviral defense(35-39). In contrast to B-DNA, left-handed Z-DNA is more prone to
81 occur in GC rich sequences and is characterized by a zig-zag shaped backbone. This DNA-
82 conformation is induced by high salt conditions, torsional stress, oxidized bases such as 8-Oxo-
83 2'-deoxyguanosine (8-oxodG) or other base modifications and further stabilized by Z-DNA
84 binding proteins(35, 40, 41). MtDNA can undergo Z-DNA formation upon mitochondrial genome
85 instability and negative supercoiling(34). Importantly, mitochondrial-derived Z-DNA is detected
86 by ZBP1 and cGAS to sustain type I IFN-responses in cardiomyocytes to promote doxorubicin-
87 induced cardiotoxicity(34).

88 Given mitochondrial damage after UV light and the type I IFN signature in autoimmune
89 photosensitive diseases, we hypothesized that UV exposure could lead to oxidized
90 mitochondria-derived cytosolic Z-DNA accumulation that is stabilized by type I IFN-induced
91 upregulation of ZBP1. This combination of Z-DNA accumulation and increased ZBP1 would
92 then lead to robust type I IFN responses in KCs. Here, we demonstrate that ZBP1 is
93 upregulated in nonlesional and lesional skin of SLE and DM patients. We provide evidence of
94 enhanced ZBP1-stabilized Z-DNA accumulation in an IFN-rich environment, which further
95 sustains IFN signaling in KCs after UV exposure via cGAS-STING activation. Knockdown of
96 ZBP1 in KCs attenuates type I IFN and IFN-stimulated gene (ISG) expression after UV, and
97 overexpression of ZBP1 in KCs results in enhanced cytosolic Z-DNA retention and type I IFN
98 signaling. Together, our data identify a novel pathway that explains how an IFN-rich
99 environment primes the skin for photosensitivity through ZBP-1-mediated Z-DNA sensing which
100 drives activation of the cGAS-STING pathway. This has important implications for treatment and
101 prevention of cutaneous and systemic flares of photosensitive autoimmune diseases.

102

103 RESULTS

104 **Ultraviolet irradiation induces mtROS-dependent type I and III IFN induction in KCs** 105 **accompanied by cytosolic Z-DNA accumulation derived from mitochondria.**

106 UV light was previously shown to cause mitochondrial damage and mitochondrial ROS (mtROS)
107 accumulation (22). However, the downstream effects of these changes have not been well-
108 characterized.

109 We hypothesized that UV-induced mtROS and release of mtDNA would lead to IFN production
110 in KCs. To test this, we irradiated N/TERT keratinocytes with UVB light and preincubated them
111 with or without mitoTEMPO, a mitochondrially targeted antioxidant (Fig. 1,A). We observed, via
112 mitoSOX Red staining, increased mtROS formation in KCs 30min after UVB exposure that was
113 inhibited by mitoTEMPO (Fig. 1,B and C). To test whether mtROS promote type I and III IFN
114 signaling after UV light, we assessed the effect of mitoTEMPO on type I and III IFN gene
115 expression. Rotenone, a complex I inhibitor and inducer of mtROS(42), was used as a positive
116 control. Both UVB and Rotenone induced a significant increase in *IFNB1* and *IFNL3* expression
117 6h after UVB which was rescued by mitoTEMPO (Fig. 1,D). MitoTEMPO also dampened
118 expression of later expressed genes, *IFNK*, *OASL* and *MX1* 24 hours after UV exposure (Fig.
119 1,E). These results indicate that mtROS are promoting type I and III IFN responses after UV in
120 KCs. To test whether mtDNA is required for UV-induced type I IFN induction, we then depleted
121 mtDNA selectively with the nucleoside 2'3'-dideoxycytosine (ddC) and observed a reduction of
122 type I IFN in a dose dependent manner (Supplemental Fig. 1,A and B). This suggests that
123 mtROS effects on mtDNA are important for UV-driven IFN production.

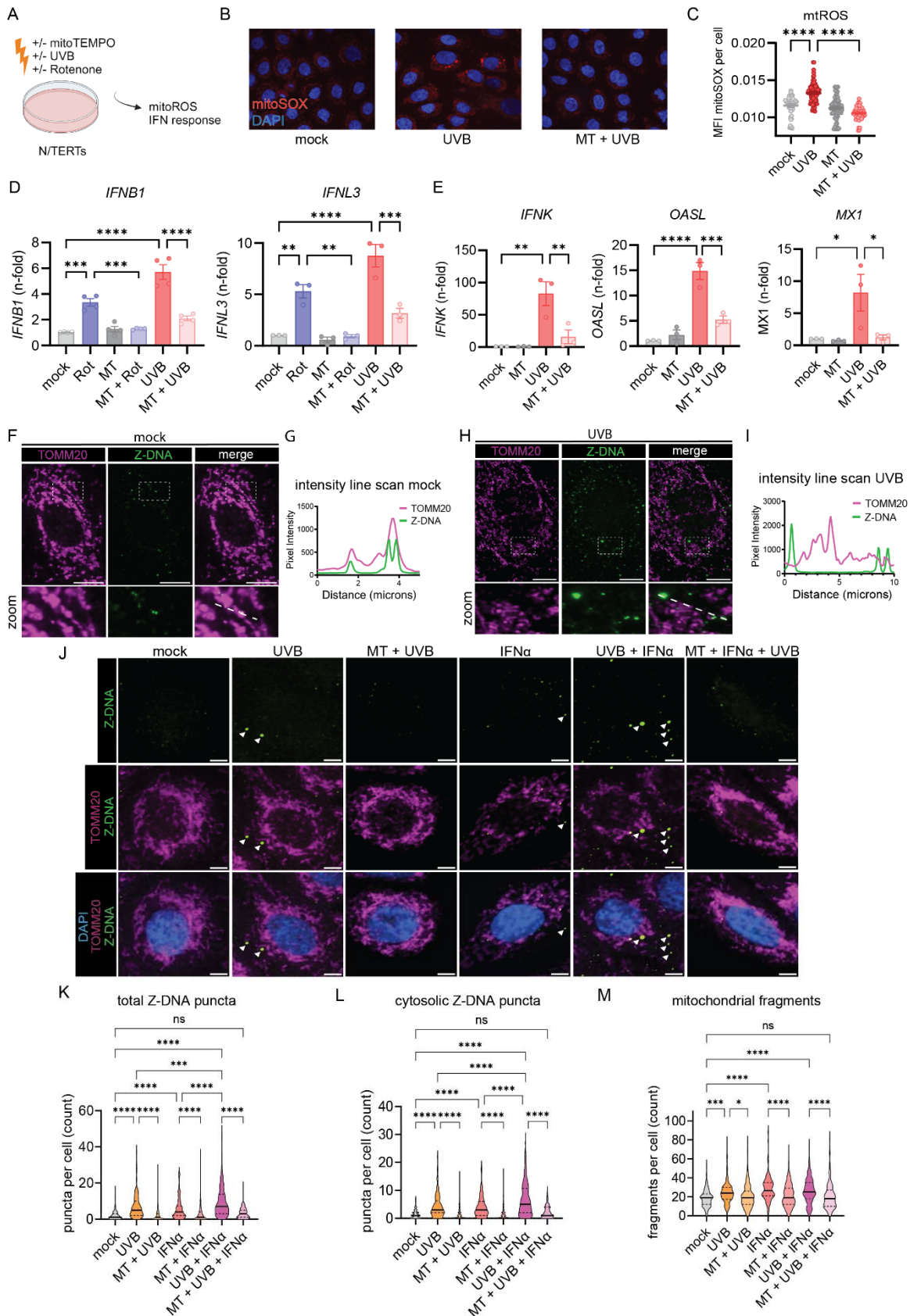
124 Oxidation of DNA and mitochondrial DNA instability can lead to formation and stabilization of
125 left-handed Z-DNA(34, 40). Therefore, we assessed Z-DNA localization and accumulation after
126 UV exposure using quantitative immunofluorescence microscopy of Z-DNA, the mitochondrial
127 outer membrane protein TOMM20 and DAPI. Utilizing a Z22 antibody which was confirmed to
128 stain Z-DNA in previous reports(34), we screened for enhanced Z-DNA staining and
129 accumulation after UVB exposure. Using super-resolved structured illumination microscopy, we
130 observed low baseline staining and mitochondrial localization of Z-DNA without stimulation (Fig.
131 1,F and G). Strikingly, after UVB we observed an increase of Z-DNA together with translocation
132 from the mitochondrial compartment into the cytoplasm with formation of prominent Z-DNA
133 puncta (Fig. 1,H and I). Further using a spinning disk confocal microscope to image larger cell
134 numbers, we observed prominent Z-DNA puncta whereas small puncta were comparatively
135 weaker (Fig. 1,J). Automated image analysis revealed that UVB significantly increased total and

136 cytosolic Z-DNA 3h after irradiation which was rescued by preincubation with mitoTEMPO (Fig.
137 1,K and L). Moreover, we observed significantly more mitochondrial fragments after UVB
138 exposure which was also rescued by mitoTEMPO (Fig. 1,M). Z-DNA was localized within the
139 mitochondrial network when cells were preincubated with mitoTEMPO (Fig. 1J), suggesting a
140 stabilization of the mitochondrial network and inhibition of Z-DNA accumulation through
141 scavenging of mtROS. We confirmed mitochondrial origin of Z-DNA by depletion of mtDNA
142 using ddC, which reduced Z-DNA intensity and puncta significantly but did not influence UVB-
143 induced mitochondrial fragmentation (Supplemental Fig. 1D-F).

144 Type I IFNs have been implicated in photosensitive responses and are responsible for an
145 autocrine loop of inflammation upon UV exposure(3, 13). To explore whether type I IFNs
146 impacted the UVB effects on mitochondrial stress and cytosolic Z-DNA accumulation, we first
147 treated N/TERTs for 16h with IFN α before irradiation to mimic a chronic type I IFN environment,
148 such as seen in SLE(3, 10-12). Via microscopy, we observed an increase in cytosolic Z-DNA
149 puncta and mitochondrial fragmentation in N/TERTs after IFN α priming alone (Fig 1. K, L). After
150 UVB exposure and IFN α priming, we observed a striking accumulation of cytosolic Z-DNA
151 puncta associated with mitochondrial fragmentation (Fig. 1,L and M). MitoTEMPO fully rescued
152 this phenotype by maintaining the mitochondrial network (Fig. 1,M). Collectively, these results
153 strongly indicate cytosolic Z-DNA accumulation derived from mitochondria upon UV-exposure is
154 dramatically increased in a type I IFN rich environment.

155

156 **Figure 1**



158 **Figure 1. UVB light causes mtROS dependent IFN responses accompanied by cytosolic**
159 **Z-DNA release derived from mitochondria.**

160 **A.** Experimental approach. **B.** Representative images from N/TERTs treated +/- mitoTEMPO (MT) +/-
161 UVB irradiation stained with MitoSOXred and Hoechst33342. **C.** Quantification of MitoSOX intensity per
162 cell using CellProfiler software. **D.** N/TERTs were treated with either rotenone, MT or UVB for 6h. Gene
163 expression of *IFNB1* (n=44) and *IFNL3* (n=3) was determined by qPCR. **E.** Gene expression of *IFNK*,
164 *MX1* and *OASL* (n=3) +/- mitoTEMPO +/- UVB 24h after UVB exposure. **F.** Representative confocal
165 microscopy from N/TERTs of TOMM20, Z-DNA, and DAPI without stimulation. **G.** Line scan analysis of
166 the line in F. **H.** Representative confocal microscopy from N/TERTs of TOMM20 and Z-DNA 3h after UVB
167 exposure. **I.** Line scan analysis of the dotted white line in H. **J.** Representative confocal images from
168 N/TERTs of TOMM20, Z-DNA, DAPI +/- mitoTEMPO, pretreatment with IFN α or 3h after UVB. Scale bar
169 5 μ m. **K-L.** Quantification of Z-DNA puncta using CellProfiler software. **M.** Mitochondrial fragments
170 (objects <1 μ m² with circularity > 0.6) using CellProfiler. Mean + SEM or violin plots with mean + quartiles
171 of n \geq 3 independent experiments. P-values were calculated using ordinary one-way ANOVA followed by
172 Sidak's multiple comparison test. *P < 0.05; **P < 0.01; ***P < 0.001; ****P < 0.0001.

173

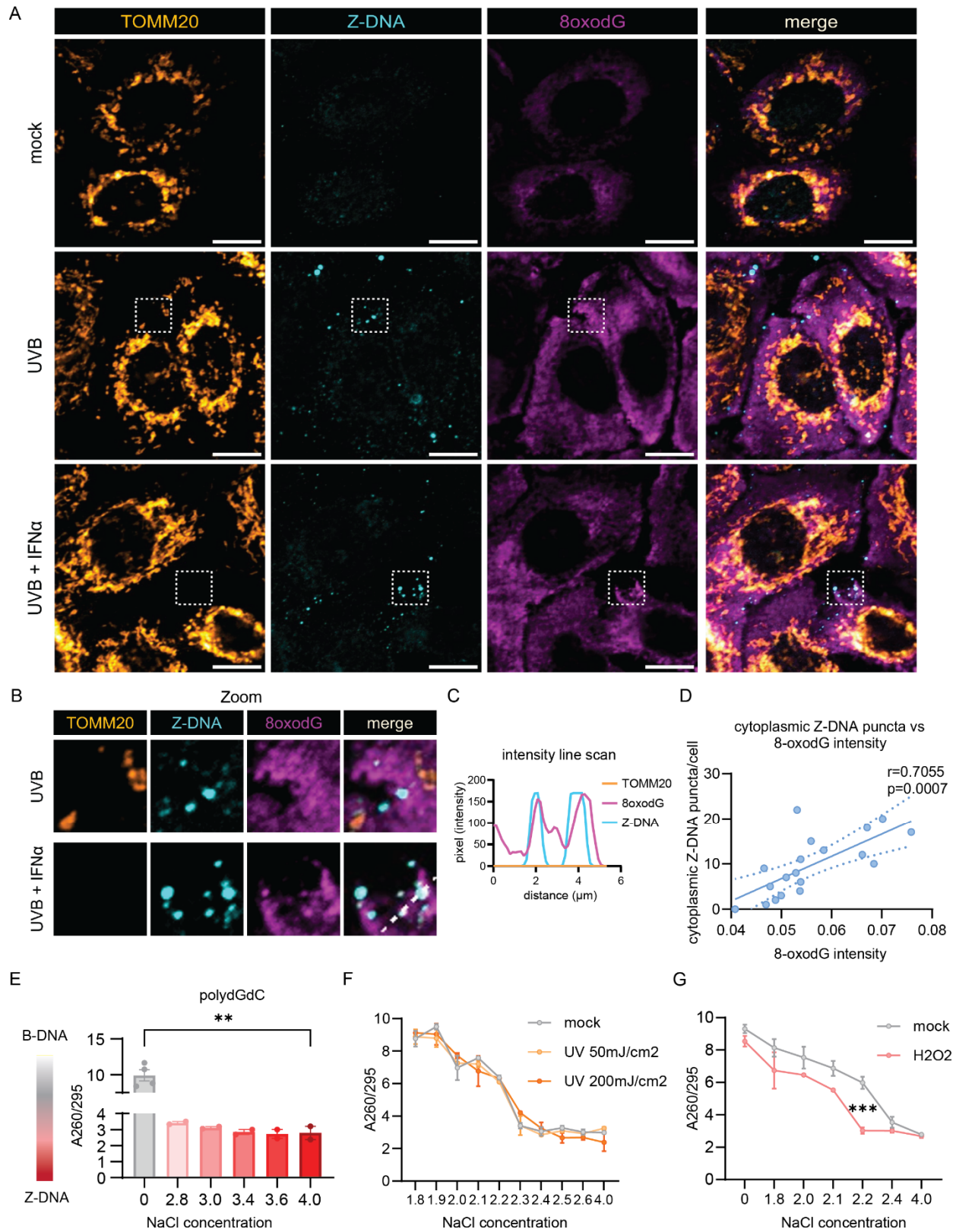
174 **UVB-induced oxidative DNA damage promotes cytosolic Z-DNA accumulation.**

175

176 Given our observations of UVB-induced mtROS and the reduction of Z-DNA by mitoTEMPO, we
177 suspected that UVB-driven oxidative mtDNA lesions would contribute to Z-DNA accumulation.
178 Previous published evidence showed that oxidative damage of Guanosine (8-Oxo-2'-
179 deoxyguanosine, 8oxodG) promotes Z-DNA formation through energetic favorability, as
180 8oxodG hinders steric formation of B-DNA and favors Z-DNA formation(40). Staining for
181 8oxodG revealed cytosolic increases upon UVB exposure whereas these lesions were partially
182 prevented by mitoTEMPO (Supplemental Fig. 1, C and D). Importantly, while 8-oxodG staining
183 was diffuse, co-staining with Z-DNA and TOMM20 revealed proximity of large Z-DNA puncta
184 with spots of enhanced 8oxodG damage outside of mitochondria after UVB exposure (Fig. 2,A
185 and B). After IFN α priming and UVB exposure, we observed that accumulation of large Z-DNA
186 puncta occurred in spots with increased 8oxodG staining (Fig. 2,A-C). There was a significant
187 positive correlation of cytosolic Z-DNA puncta and 8oxodG intensity per cell, suggesting 8oxodG
188 damage promotes Z-DNA conformation (Fig. 2,D). In addition, mitochondrial fragmentation after
189 IFN α priming and UVB exposure exhibited a similar positive correlation with cytosolic Z-DNA
190 accumulation (Supplemental Fig. 3,A-E). These results suggest cytosolic Z-DNA accumulation
191 is associated with mitochondrial fragmentation and oxidative DNA damage.

192 To test whether Z-DNA formation required oxidative lesions, we utilized an assay that examines
193 Z-DNA formation in polydGdC oligos induced by high [NaCl](43, 44). Z-DNA conformation under
194 high salt was confirmed using the A260/295 ratio which is significantly lower in Z-DNA
195 compared to the B conformation (Fig. 2,E)(43, 45). To test whether UVB exposure would
196 directly lead to Z-DNA accumulation, we irradiated polydGdC with low (50mJ/cm²) and high
197 (200mJ/cm²) doses of UVB light. We did not observe direct induction of Z-DNA conformation
198 upon UVB exposure (Fig. 2,F), suggesting no direct oxidative DNA damage at the doses used in
199 our *in vitro* system. However, induction of oxidation by H₂O₂ permitted Z-DNA formation at
200 significantly lower concentrations of NaCl (Fig. 2,G). These results suggest that UVB light
201 promotes Z-DNA conformation indirectly by accumulation of oxidative DNA damage. We then
202 examined whether IFN α would increase cytoplasmic Z-DNA by augmenting mitochondrial or
203 cellular ROS. Surprisingly, IFN α did not enhance ROS generation, suggesting that IFN α -
204 induced increase of cytoplasmic Z-DNA accumulation is independent of ROS generation
205 through IFN α (Supplemental Fig. 4,A and B).

206 **Figure 2.**



207

208

209

210 **Figure 2. UVB promotes Z-DNA formation via oxidative DNA damage**

211 **A.** Representative confocal images of the mitochondrial outer membrane (TOMM20), Z-DNA and 8oxodG
212 in N/TERTs at baseline, 3h after UVB exposure with or without IFN α preincubation for 16h. Scale bar
213 10 μ m. **B.** Magnified region from (A) highlighting proximity and colocalization of Z-DNA with intense
214 8oxodG staining in areas outside of mitochondria. **C.** Representative line scan from Z-DNA puncta in (B)
215 highlighting the absence of TOMM20 in spots of Z-DNA accumulation. **D.** Correlation of the Z-DNA puncta
216 per cell with matched average 8oxodG per cell. **E.** Change of A260/295 as a measure of B-DNA (high
217 ratio~10) vs Z-DNA (lower ratio of ~3) formation is graphed comparing low salt vs. high salt conditions
218 after 2h at 37°C. **F.** Naked polydGdC was irradiated with indicated UVB doses and incubated in indicated
219 [NaCl] as in E. to induce Z-DNA. No shift to a lower ratio in lower [NaCl] was detected after UVB light
220 exposure.

221 **G.** To test the effect of oxidation on propensity for Z-DNA formation, polydGdC was treated with H₂O₂
222 (1mM) for 2h at 37°C and subjected to varying salt concentrations as in E. Buffers with indicated NaCl
223 and H₂O₂ without DNA served as blanks for the assay.

224

225 **ZBP1 is overexpressed in photosensitive autoimmune skin diseases and correlates with**
226 **type I IFN scores.**

227

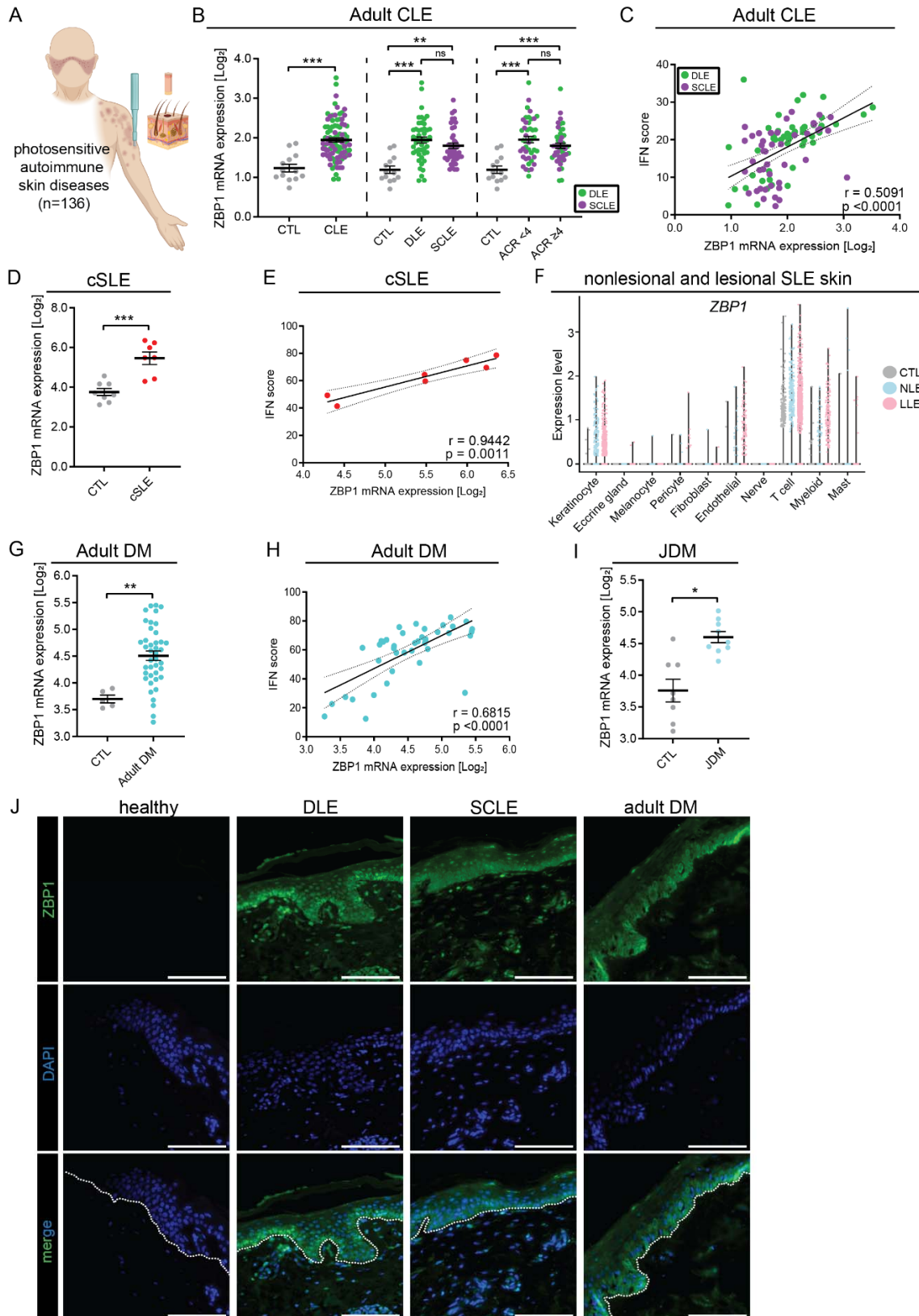
228 Autoimmune photosensitive diseases share a cutaneous IFN signature in lesional and non-
229 lesional skin that can be further induced after UV exposure to promote chronic cutaneous
230 inflammation(1, 2, 10-13, 25). As UVB-mediated cytosolic mtDNA in Z form is promoted by type
231 I IFNs (Fig. 1, J-L), we hypothesized that the chronic type I IFN high environment in
232 autoimmune photosensitive diseases may contribute to this sustained inflammation. Intriguingly,
233 Z-DNA conformation can be stabilized by the IFN-regulated gene Z-DNA binding protein 1
234 (*ZBP1*)(34-36), so we chose to further examine the role of *ZBP1* in autoimmune photosensitive
235 diseases (Fig. 3,A). Strikingly, *ZBP1* expression was significantly upregulated in a large cohort
236 of CLE lesional skin biopsies (n=90) compared to healthy controls (CTL) (n=13) (Fig. 3,B). This
237 upregulation was independent of CLE subtype and presence or absence of systemic disease
238 (Fig. 3,B). Furthermore, *ZBP1* expression correlated significantly with IFN scores in CLE,
239 suggesting its upregulation to be a phenomenon of cutaneous IFN expression rather than
240 specific systemic clinical features (Fig. 3,C). We confirmed these results in microarray datasets
241 from patients with childhood SLE (cSLE) (n=7), where we observed significant upregulation of
242 *ZBP1* gene expression compared to CTL (n=8) and significant correlation with the cutaneous
243 IFN score (Fig. 3,D and E). To assess nonlesional *ZBP1* expression in the skin and identify
244 which cells are expressing *ZBP1*, we utilized our single-cell-sequencing dataset of lupus
245 patients (n=14) compared to CTL (n=14)(12). We confirmed robust upregulation of *ZBP1* in
246 nonlesional and lesional keratinocytes compared to CTL (Fig. 3,F). There was also a similar, but
247 weaker, trend in cutaneous myeloid cells and endothelial cells; *ZBP1* expression was mostly
248 absent in fibroblasts, melanocytes, and mast cells (Fig. 3,F).

249 Further analysis of adult DM (n=30) and JDM (n=9) compared to CTL (n=8 and n=5,
250 respectively) revealed significant cutaneous *ZBP1* upregulation in DM and JDM with significant
251 correlation of *ZBP1* expression with the IFN score in adult DM (Fig. 2,G-I). In JDM, we were
252 underpowered to observe a significant correlation between IFN score and *ZBP1*, but there was
253 a similar trend (Supplemental Fig. 5,A). The expression of *ZBP1* in lupus skin samples neither
254 correlated with autoantibody status, disease activity nor with age (Supplemental Fig. 5, B and
255 C), suggesting upregulation of *ZBP1* is independent of these patient characteristics.

256 Next, we examined the protein expression of *ZBP1* by staining skin samples from nonlesional
257 and lesional lupus and DM skin. As expected, we observed increased *ZBP1* in nonlesional and
258 lesional discoid lupus erythematosus (DLE), subacute cutaneous lupus erythematosus (SCLE)

259 and DM epidermis compared to CTL, where ZBP1 was basically undetectable (Fig. 3,J).
260 Notably, ZBP1 was highest expressed in the basal layer of the epidermis. In sum, these results
261 indicate epidermal upregulation of ZBP1 in nonlesional and lesional skin of autoimmune
262 photosensitive diseases correlates with cutaneous IFN signatures and suggests that ZBP1 may
263 be important for downstream immune responses in adult and pediatric CLE, SLE and DM skin.
264

265 **Figure 3**



267 **Figure 3. ZBP1 is overexpressed in the epidermis of autoimmune photosensitive**
268 **diseases.**

269 **A.** Graphical representation of data acquisition from lesional skin microarrays.
270 **B.** *ZBP1* expression in lesional cutaneous lupus (CLE) (n=90) compared to healthy control (CTL) (n=13)
271 (left), by lesion subtype (discoid lupus erythematosus (DLE) or subacute cutaneous lupus erythematosus
272 (SCLE), middle) and based on the presence or absence of systemic lupus via >4 1997 ACR criteria
273 (right). **C.** Correlation of *ZBP1* expression in CLE with IFN score, linear regression. **D.** *ZBP1* expression in
274 childhood onset systemic lupus erythematosus (cSLE, n=7) compared to CTL (n=8). **E.** Correlation of
275 *ZBP1* expression with IFN score in cSLE. **F.** Violin plots showing *ZBP1* expression from scRNA
276 sequencing across cutaneous cell types from nonlesional lupus skin (NLE, n=14), lesional lupus skin
277 (LLE, n=14) compared to CTL (n=14). **G.** Expression of *ZBP1* in adult dermatomyositis (DM) (n=41) and
278 **H.** Correlation with IFN score by linear regression. **I.** *ZBP1* expression in juvenile dermatomyositis (jDM,
279 n=9) compared to CTL (n=8). **J.** Representative images of tissue immunofluorescence of *ZBP1* in CTL (n=
280 7), DLE (n=8), SCLE (n=5) and DM (n=6). Dotted white line indicates the dermo-epidermal junction. Scale
281 bar =100µm. Mean + SEM. * = $q < 0.05$; ** = $q < 0.01$; *** = $q < 0.0001$, by Student's unpaired t-test.

282

283 **Lupus KCs exhibit strong baseline and UV-induced cytosolic Z-DNA compared to CTL.**

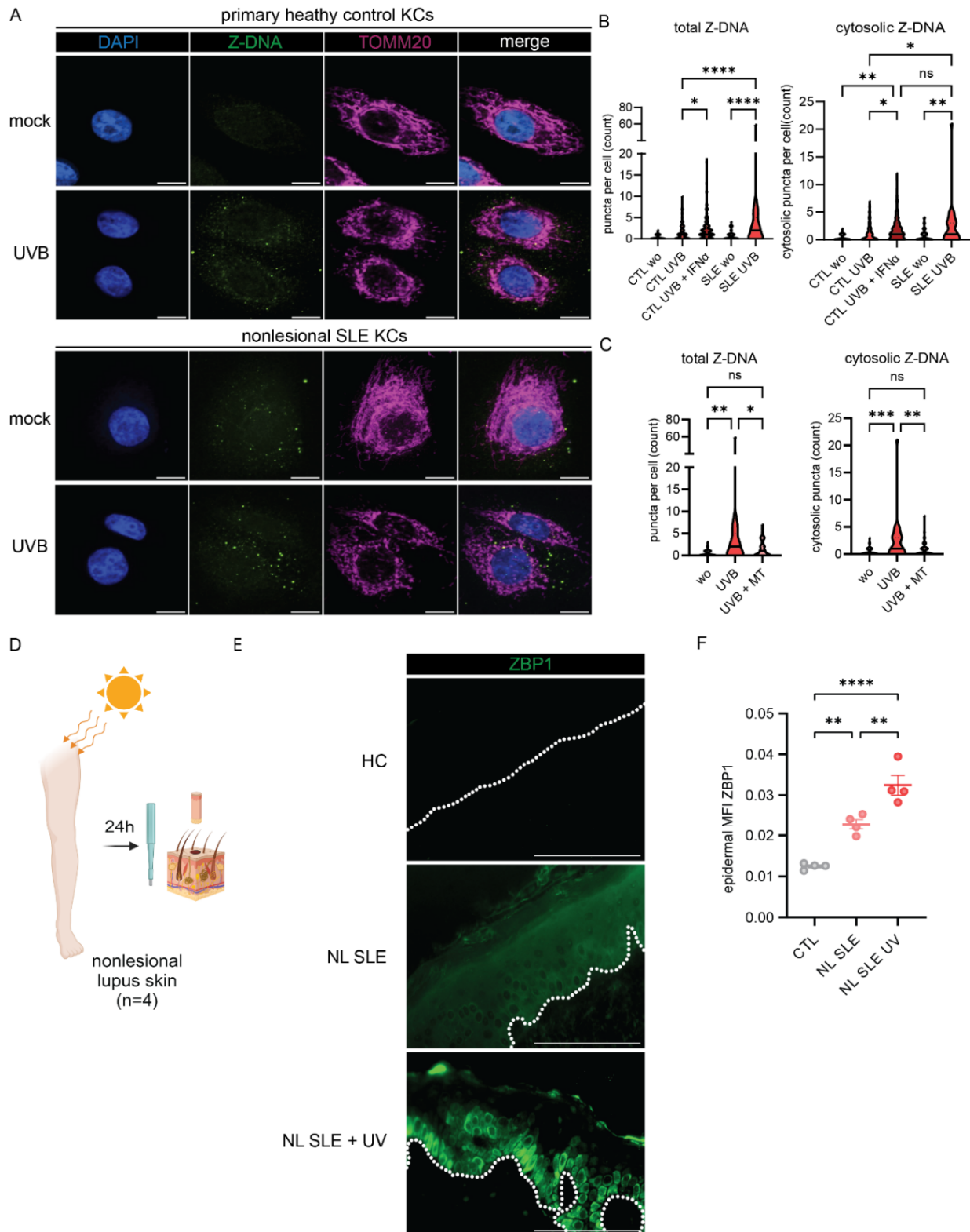
284

285 Given enhanced IFN signaling and significant upregulation of ZBP1 in lupus KCs, we quantified
286 cytosolic Z-DNA puncta in CTL and lupus KCs at baseline and after UVB exposure (Fig. 4,A). At
287 baseline, CTL KCs exhibited Z-DNA staining primarily within the mitochondrial network (Fig.
288 4,A). After UVB exposure, we observed the expected cytosolic Z-DNA accumulation in CTL KCs
289 (Fig. 4,A and B). Strikingly, lupus KCs exhibited enhanced total and cytosolic Z-DNA puncta at
290 baseline that were significantly increased after UVB with formation of multiple large cytosolic
291 puncta (Fig 4,A and B). Preincubation of CTL KCs with IFN α promoted enhanced cytosolic Z-
292 DNA accumulation after UVB exposure, comparable with nonlesional lupus KCs after UVB
293 alone, suggesting that the known chronic IFN loop in SLE KCs(3, 13) stabilizes Z-DNA,
294 potentially through the ISG ZBP1. Surprisingly, Z-DNA accumulation in the cytosol after UVB
295 exposure of lupus KCs was prevented by preincubation with mitoTEMPO, which led to
296 stabilization of Z-DNA within the mitochondrial network (Fig. 4,C).

297 As UVB treatment of KCs upregulates type I and type III IFNs, we examined whether
298 mitoTEMPO also decreased UV-induced IFN gene expression in lupus primary KCs. In line with
299 our microscopy data, we observed that mitoTEMPO led to significant downregulation of *IFNB1*,
300 *IFNL3* and ISGs after UVB exposure (Supplemental Fig. 6,A and B). Baseline and UVB-induced
301 cellular ROS were not increased in SLE KCs compared to primary HC KCs (Supplemental Fig.
302 6,C). To further assess the role of ZBP1 *in vivo*, we assessed ZBP1 protein expression in lupus
303 nonlesional skin samples collected by biopsy 24 hours after irradiation with a minimal erythema
304 dose of UVB (Fig. 4,D). Strikingly, in addition to upregulation of ZBP1 in nonlesional SLE skin
305 compared to CTL, we observed enhanced expression and cytosolic localization of ZBP1 in the
306 basal epidermis of nonlesional SLE skin after UV exposure (Fig. 4,E and F), suggesting a role
307 for ZBP1 in UV-mediated responses in SLE *in vivo*. Together, these results show activation of
308 the Z-DNA/ZBP1 pathway in SLE compared to HC skin after UV exposure.

309

310 **Figure 4**



311

312

313

314 **Figure 4. Nonlesional lupus keratinocytes exhibit cytosolic Z-DNA accumulation at**
315 **baseline and after UVB exposure that is prevented by mitoTEMPO.**

316 **A.** Representative images of confocal microscopy staining for Z-DNA, TOMM20 and counterstaining with
317 DAPI at baseline and after UVB exposure and preconditioning with IFN α (1000U/ml for 16h prior to UVB
318 exposure) in primary healthy control KCs (n=4) and SLE KCs (n=3). **B-C.** Quantification of total and
319 cytosolic Z-DNA puncta after UVB with or without preincubation with mitoTEMPO or IFN α using
320 CellProfiler. **D.** Healthy controls (HC), SLE patients +/- UVB (n=4 each group) were biopsied 24h after UV
321 exposure. **E.** Representative images of ZBP1 staining in HC, nonlesional SLE skin (NL SLE) and NL SLE
322 after UV exposure. Dotted white line indicates the dermo-epidermal junction. Scale bar =100 μ m **F.**
323 Quantification of mean fluorescence intensity (MFI) of epidermal ZBP1 using open source CellProfiler
324 software. Ordinary one-way ANOVA followed by Sidak's multiple comparison test. Mean and SEM.
325 *P<0.05, **P<0.01, ***P<0,001, ****P<0.0001.

326

327 **Z-DNA has stronger immunostimulatory properties than B-DNA to sustain STING-**
328 **dependent IFN responses in human KCs.**

329

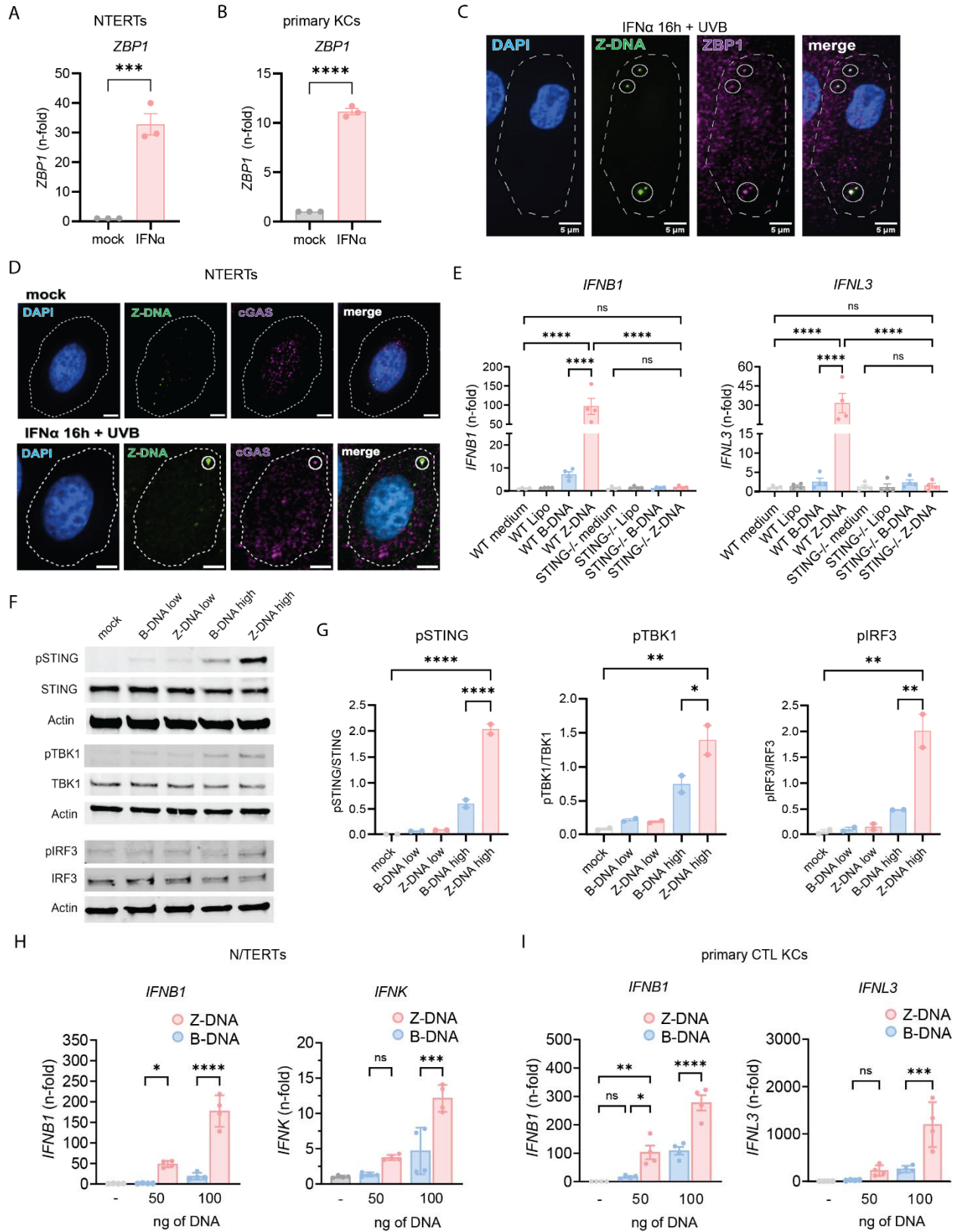
330 ZBP1 was recently described to bind cGAS within the cytoplasm resulting in bridging of Z-DNA
331 to cGAS and subsequent STING activation and sustained type I IFN responses(34). Hence, we
332 next assessed the effects of ZBP1 and DNA in the Z conformation on IFN activation in KCs.

333 First, we confirmed upregulation of *ZBP1* after IFN α treatment in N/TERTs and primary KCs
334 (Fig. 5,A and B). We then assessed co-localization of Z-DNA and ZBP1 after UVB with and
335 without IFN α priming. As shown in Fig. 5C, UV treatment induced co-localization of Z-DNA
336 puncta and ZBP1 in the cytoplasm, and this was expectedly enhanced when cells were first
337 primed with IFN α . These data confirmed previous study results that ZBP1 and Z-DNA form a
338 cytosolic complex and that type I IFNs enhance this through upregulation of ZBP1 and
339 increased Z-DNA formation(34).

340 cGAS-dependent type I IFN responses have been described after UVB(24). Small Z-DNA
341 puncta, which were primarily localized within the mitochondria (Fig. 1,F), did not colocalize with
342 cGAS (Fig. 5,D). After UVB, we observed both cytoplasmic localization of cGAS as well as
343 colocalization with large Z-DNA puncta (Fig. 5,D, Supplemental Fig. 7,A and B). This suggests
344 that cGAS joins the complex of ZBP1 and Z-DNA within the cytosol after UVB exposure. To test
345 whether Z-DNA signaling is cGAS-STING dependent, we transfected WT and STING^{-/-}
346 N/TERTs with polydGdC, which is known to form Z-DNA conformation upon binding to positively
347 charged Lipofectamine(46) and compared it to transfection of an equal amount of B-DNA. Both
348 *IFNB1* and *IFNL3* expression were completely abrogated in STING^{-/-} KCs compared to mock
349 knockout N/TERTs (Fig. 5,F). Intriguingly, we observed stronger activation of *IFNB1* and *IFNL3*
350 expression 6h after Z-DNA transfection compared to B-DNA in WT KCs. We confirmed these
351 results by Western Blot of pSTING, pTBK1 and pIRF3, revealing robust activation of this
352 pathway by Z-DNA transfection (Fig. 5,G and H). We then assessed type I and type III IFN
353 production in response to B- or Z-DNA and identified a striking difference in the upregulation of
354 IFN genes and ISGs in Z-DNA transfected KCs (Fig. 5,J, Supplemental Fig. 8,A and B). This
355 was confirmed in primary CTL KCs (Fig. 5,K). Interestingly, *ZBP1* expression was also induced
356 to a significantly greater extent by Z-DNA compared to B-DNA transfection (Supplemental Fig.
357 8,A and B).

358 Together, these results confirm interaction of Z-DNA with ZBP1 in human primary keratinocytes
359 and identify Z-DNA as more immunostimulatory compared to B-DNA in a cGAS-STING
360 dependent fashion.

362 **Figure 5**



363

364

365 **Figure 5. Z-DNA binds to ZBP1, activates the cGAS-STING pathway and has stronger**
366 **immunostimulatory properties than B-DNA.**

367 **A-B.** Gene expression of *ZBP1* after IFN α stimulation in N/TERTs (**A.**) and primary healthy control KCs
368 (**B.**) compared to β -Actin. **C.** Representative image of confocal microscopy from N/TERTs preincubated
369 with IFN α (1000U/ml) and then irradiated with UVB exposure stained for Z-DNA, ZBP1, and DAPI 3h after
370 UVB exposure. Scale bar 5 μ m. **D.** Representative images of IFN α -treated N/TERTs stained for Z-DNA,
371 cGAS and DAPI 3h after UVB exposure. Cellular outline was drawn based on CellTrackerRed
372 counterstain. **E.** Gene expression at 6h of indicated genes from N/TERTs and STING KO N/TERTs
373 treated with Lipofectamine2000 alone or transfected with Z-DNA or B-DNA (500ng/ml). **F.** Representative
374 Western Blot (n=2) of indicated proteins from N/TERTs transfected with 50ng (low) or 500ng (high) of Z-
375 DNA (polydGdC) or B-DNA using Lipofectamine 2000. Lysates harvested 4h after transfection. **G.**
376 Quantification of the abundance of pSTING, pIRF3, and pTBK1 relative to unphosphorylated proteins in
377 transfected KCs. **H.** N/TERTs were transfected as in E and gene expression was measured 6h after DNA
378 transfection (n=3). **I.** Primary control KCs (n=3) were transfected and analyzed as in H. Unpaired t-test
379 and Ordinary one-way ANOVA followed by Sidak's multiple comparison test. Mean and SEM. *P<0.05,
380 **P<0.01, ***P<0,001, ****P<0.0001.

381

382 **ZBP1 is required for IFN signaling after UVB exposure and its upregulation recapitulates**
383 **an autoimmune photosensitive phenotype in KCs.**

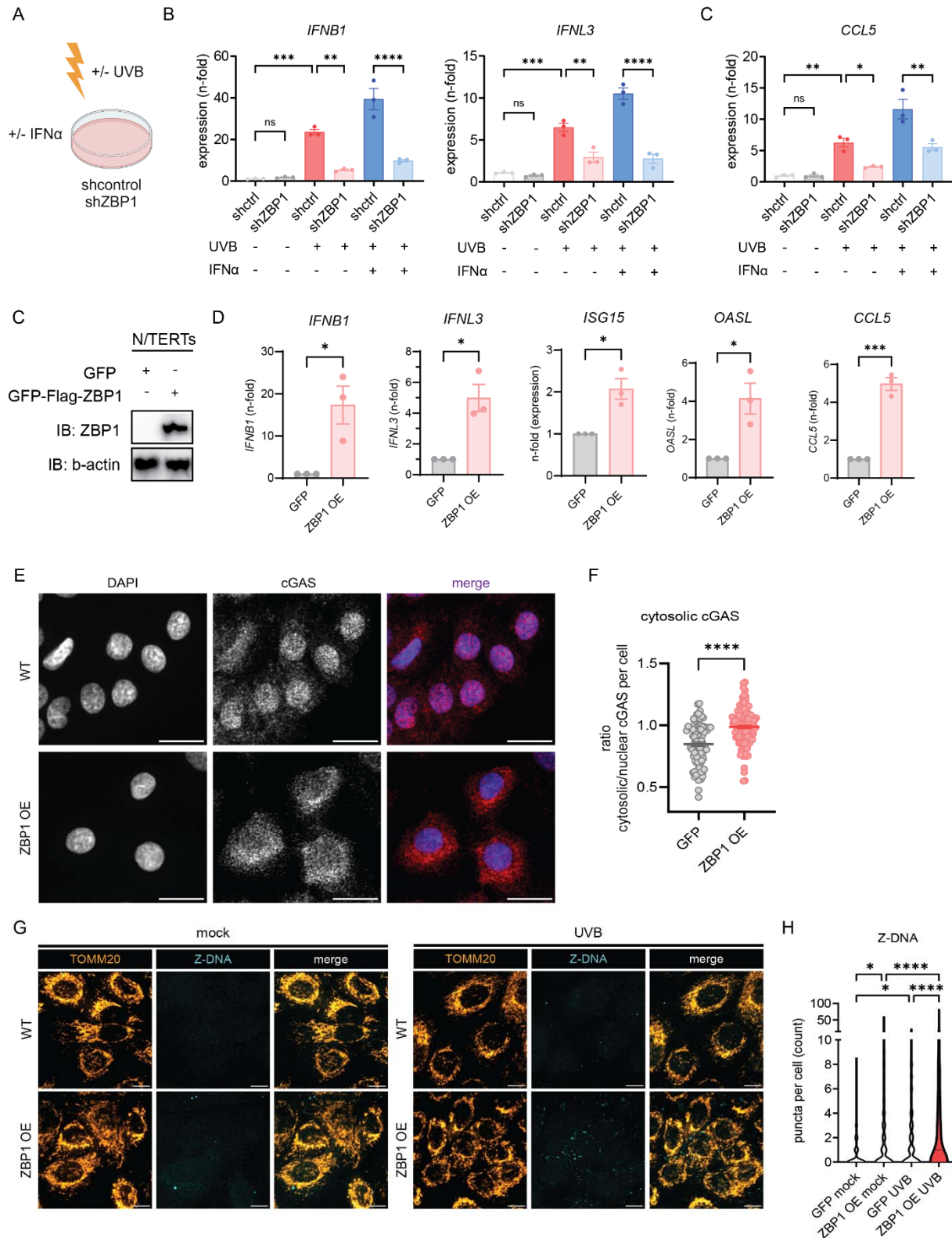
384

385 Given upregulation of ZBP1 by IFN α and stronger Z-DNA accumulation after UVB in IFN α -
386 primed KCs, we next wanted to explore whether knockdown of ZBP1 reduced UVB-induced
387 type I IFN responses, especially in an IFN-rich environment. We thus generated a knockdown of
388 *ZBP1* using shRNA in N/TERTs (Fig. 6,A, Supplemental Fig. 9,A). After UV exposure, KCs
389 deficient in ZBP1 showed less type I and III IFN activation compared to controls (Fig. 6,B).
390 Priming with IFN α prior to UVB exposure led to significant upregulation of *IFNB1* and *IFNL3*
391 gene expression in shcontrol KCs whereas this enhancement was absent in shZBP1 KCs (Fig.
392 6,B). The robust upregulation of the ISG *CCL5* expression following priming with IFN α prior to
393 UV was also dramatically decreased in the absence of ZBP1 (Fig. 6,C). These results suggest
394 that ZBP1 is required for UV-driven IFN responses and is particularly crucial for the effects of
395 type I IFN priming on cGAS/STING activation and IFN production.

396 ZBP1 is increased in the epidermis of adult and childhood SLE as well as in adult and juvenile
397 DM. To mimic the phenotype observed in these autoimmune photosensitive diseases, we
398 generated a GFP-ZBP1-FLAG tagged KC cell line in N/TERTs and compared it to a N/TERT
399 line expressing GFP alone (Fig. 6,D, Supplemental Fig. 9, B and C). ZBP1 was primarily
400 expressed in the cytoplasm in the overexpressing cell line (Supplemental Fig. 9,D).
401 Upregulation of ZBP1 was confirmed by Western Blot (Fig. 6,D). We next tested for IFN gene
402 expression in GFP-ZBP1-FLAG KCs. Strikingly, we observed significant upregulation of both
403 type I and III IFNs as well as ISGs in GFP-ZBP1-FLAG KCs compared to GFP KCs without
404 additional stimulation (Fig. 6,E). In addition, confocal microscopy revealed cytosolic localization
405 of cGAS in ZBP1 overexpressing KCs, consistent with its activation (Fig. 6,G). We then wanted
406 to know whether overexpression of ZBP1 was sufficient to increase cytosolic Z-DNA at baseline
407 and after UV exposure. Indeed, cytosolic Z-DNA was increased at baseline in the ZBP1
408 overexpressing KCs compared to controls (Fig. 6,H and I). These results are in line with our
409 previous observations that IFN α treatment alone can increase cytosolic Z-DNA (Fig. 1,J-L). After
410 UVB exposure, we observed massive cytosolic Z-DNA accumulation in GFP-ZBP1-FLAG KCs
411 compared to GFP control (Fig. 6,H and I). Importantly, mitochondrial fragmentation did not differ
412 between GFP-ZBP1-FLAG KCs compared to GFP control (Supplemental Fig. 9, E). These data
413 suggest that ZBP1 overexpression is sufficient to promote Z-DNA stabilization and its
414 downstream IFN signaling but does not affect mitochondrial health per se.

415 Together, these results indicate that upregulation of ZBP1 is sufficient to stabilize Z-DNA and
416 promote STING activation. Importantly, ZBP1 is required for pro-inflammatory effects of type I
417 IFNs on UV-mediated STING activation. Upregulation of ZBP1 recapitulates the phenotype
418 observed in autoimmune photosensitivity and explains the propensity for inflammatory rather
419 than immunosuppressive responses upon UV exposure in a high type I IFN environment (Fig.
420 7).
421

422 **Figure 6**



423

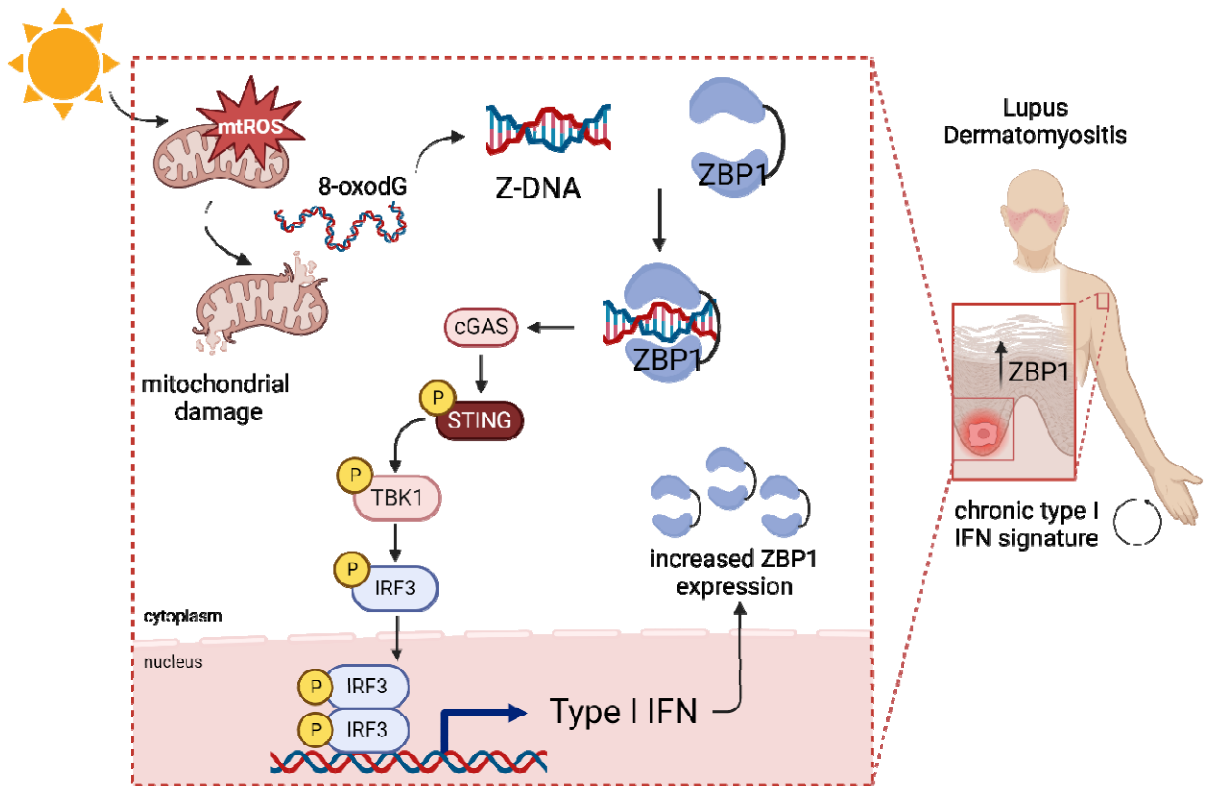
424

425 **Figure 6. ZBP1 regulates UVB-induced type I and III IFN responses in human**
426 **keratinocytes.**

427 **A-B.** Knockdown of ZBP1 in N/TERTs was performed using a lentivirus expressing either shRNA
428 targeting Human ZBP1 or shcontrol. Baseline, UV, and UV+IFN α induced gene expression were
429 assessed for **(A.)** Type I and III IFN (6h after UVB) and **(B.)** CCL5, a known ISG (24h after UVB); n=3 **C.**
430 Generation of GFP/3XFLAG-tagged N/TERTs with overexpression of ZBP1 compared to GFP-tag only.
431 **D.** IFN genes and ISGs were assessed by RT-qPCR at baseline in ZBP1 overexpressing cells (ZBP1 OE)
432 or GFP-expressing control N/TERTs (GFP). **E.** Representative greyscale and merged images of confocal
433 microscopy from N/TERTs with GFP or GFP-ZBP1 N/TERTs for cGAS (red) and DAPI (blue). Scale bar
434 20 μ m. **F.** Quantification of cytosolic cGAS using ratio of cGAS MFI in the cytosol versus nuclear cGAS
435 MFI using CellProfiler. **G.** Representative confocal images of GFP-tagged N/TERTs or ZBP1
436 overexpressing N/TERTs of TOMM20 and Z-DNA at baseline and 3h after UVB exposure. Scale bar
437 10 μ m. Ordinary one -way ANOVA followed by Sidak's multiple comparison test. Mean and SEM.
438 *P<0.05, **P<0.01, ***P<0,001, ****P<0.0001.

439

440 **Figure 7.**



441

442 **Figure 7. Graphical abstract**

443 UV light promotes mitochondrial ROS formation and mitochondrial damage which results in release of
444 oxidized DNA that can promote Z-DNA conformation. In lupus and dermatomyositis skin, Z-DNA is
445 stabilized by ZBP1 and further activates the cGAS-STING-TBK1-IRF3 pathway to promote type I IFN
446 secretion. This results in more ZBP1 expression, explaining the autocrine loop of type I IFN that is
447 observed in photosensitive autoimmune diseases after UV light.

448

449 **Discussion**

450

451 Here, we describe a novel pathway contributing to photosensitive responses in autoimmune
452 patients. In KCs, chronic IFN α exposure results in upregulation of ZBP1, which stabilizes UVB-
453 induced immunostimulatory Z-DNA derived from oxidized mitochondrial DNA leading to STING-
454 dependent type I and type III IFN production. Knockdown of ZBP1 abrogated IFN responses in
455 KCs and overexpression of ZBP1 resulted in spontaneous IFN activation and Z-DNA
456 accumulation in the cytoplasm. Indeed, our data support a growing list of studies that implicate
457 mitochondrial DNA sensing in a variety of autoimmune diseases including SLE and DM; here,
458 we add skin responses to the list of affected organs and provide the first description for a role of
459 ZBP1 in this process(26-29, 31, 32).

460 The effects of mtDNA oxidation and their contributions to SLE are numerous. Our data show
461 that oxidative DNA lesions after UV exposure promote Z-DNA conformation. In lupus, oxidized
462 mtDNA promotes IFN signaling in neutrophil extracellular traps(28, 29). Furthermore, oxidized
463 mtDNA induces a lupus like phenotype in mice, and mtDNA derived from mitochondria-
464 containing red blood cells drives IFN signaling in lupus monocytes(31, 47). Whether Z-
465 conformation contributes to these phenotypes will require additional study. Oxidation of genomic
466 DNA confers resistance to degradation by TREX1 and potentiates immunostimulation(23).
467 Further, oxidized DNA in the skin of lupus patients colocalizes with the ISG MX1 but evidence
468 that lupus skin shows higher amounts of oxidative DNA lesions is lacking. Our data do not
469 support a role for type I IFN in promotion of ROS in keratinocytes. Rather, our model suggests
470 that oxidized DNA damage by UV results in Z-DNA conformation and that stabilization of the Z-
471 DNA by the ISG ZBP1 is critical to promote more inflammation in diseases such as SLE and
472 DM.

473 Morphological changes in mitochondria have been associated with mtDNA damage, mitophagy
474 and recently, mitochondrial fragmentation due to apoptotic stress was associated with mtDNA
475 release during senescence(48). In our data, we observed a correlation of cytosolic Z-DNA
476 accumulation and mitochondrial fragmentation, indicating mitochondrial dynamics may regulate
477 Z-DNA signaling. It is therefore intriguing to hypothesize that Z-DNA accumulation could also be
478 involved in mtDNA-driven inflammatory states such as cellular senescence.

479 Our data also prompt the question of whether oxidized mtDNA from other cell types, including
480 immune cells, is likely to transition to Z-DNA and whether Z-DNA sensing may be a central
481 mechanism of the disease-promoting IFN signaling in SLE. Upregulation of ZBP1 is not only
482 observed in lupus skin but also in peripheral blood of SLE patients(49). Whether this

483 upregulation is functionally relevant and regulates responses to oxidized mtDNA in immune
484 cells should be further investigated.

485 Autoantibodies against nucleic acids are a hallmark of SLE development(50). Interestingly, SLE
486 patients exhibit autoantibodies against Z-DNA; this was described many years ago and
487 confirmed recently(51, 52). However, the substrates for generation of these antibodies have not
488 been studied. Given our data, it is intriguing to propose that Z-DNA derived from UV-irradiated
489 keratinocytes could also serve as an autoantigen and drive the adaptive immune response,
490 especially in the context of UV-mediated systemic disease flares.

491 Epidermal type I IFN secretion including IFN β and IFN κ was shown to drive immune responses
492 and enhanced cell death in the skin after UVB exposure(11). Other previous studies on
493 mechanisms of photosensitivity in lupus patients were performed in monogenic lupus where
494 cGAS-dependent IFN signaling has been described in TREX1 deficiency(23, 25). Nuclear DNA
495 fragments can be released during DNA repair processes and release of nuclear DNA due to
496 rupture of the nuclear envelope can further activate cGAS dependent IFN expression(53-55).
497 This has been described in senescence and genetic instability syndromes such as Bloom
498 syndrome(53, 55-57). Whether nuclear DNA contributes to STING signaling in autoimmune
499 photosensitivity seems unlikely based on our data and others'. First, the rate of skin cancer in
500 autoimmune photosensitive diseases is not comparable to those with DNA repair deficiencies,
501 indicating no persistence of increased nuclear DNA damage(58). Second, type I IFN may
502 increase repair of cyclobutane pyrimidine dimers, the main nuclear DNA lesion upon UV light
503 exposure(59). Third, mtDNA is more susceptible to oxidative modifications due to close
504 proximity to ROS production, a lack of protective histones and insufficient DNA repair
505 mechanisms compared to nuclear DNA(19, 22, 60). Fourth, we did not observe enhanced Z-
506 DNA formation within the nucleus nor in micronuclei after UV exposure, which can activate
507 cGAS during genetic instability(61). Finally, depletion of mitochondrial DNA abrogated UVB-
508 mediated IFN upregulation.

509 We identified a critical role for ZBP1 in Z-DNA sensing and stabilization after UV exposure.
510 ZBP1 is involved in multiple cellular processes in both antiviral defense via activation of the NF-
511 κ B pathway and induction of PANoptosis(36, 37, 62-65). Furthermore, it can sustain IFN
512 signaling after release of mitochondrial Z-DNA after Doxorubicin(34, 35). So far, previous
513 investigations utilized mostly murine data and investigated cell death pathways: Within the skin,
514 murine ZBP1 was shown to drive necroptosis and autoinflammation only in RIPK1 deficient
515 mice(39). In presence of RIPK1, necroptotic signaling of ZBP1 is inhibited and recent evidence
516 revealed that ZBP1 interacts with RIPK1 to sustain IFN signaling in a STAT1 dependent

517 manner(34, 39). In our model, cells with overexpression of ZBP1 displayed a spontaneous type
518 I IFN signature without a significant increase of cell death at baseline. We surmise that this may
519 indicate that in an interferon-rich environment, as is seen in autoimmune photosensitive
520 diseases, the primary role of ZBP1 is to bind ZDNA and regulate IFN signaling. It is possible
521 that a second stimulus (such as inhibition of caspase-8 or downregulation of RIPK1) is needed
522 to confer cells towards a cell death phenotype rather than innate immune activation. Previous
523 data of our laboratory found that indeed, IFN α priming promotes apoptotic death rather than
524 other cell death pathways (Loftus *et al.*, under review). Thus, the IFN milieu could act as a
525 “switch” which toggles the function of ZBP1 towards IFN secretion and apoptosis and away from
526 panoptotic cell death. In contrast, diseases with increases in IFN γ show enhanced necroptosis
527 of keratinocytes(66). Of note, ZBP1 can also activate the inflammasome via interaction with
528 AIM2, ASC and pyrin to result in IL1 β secretion(67). Further evidence is needed to understand
529 the role of ZBP1 in inflammasome and cell death pathways in the skin.

530 Other photosensitive disorders not examined in this paper include porphyrias which are driven
531 by the accumulation of porphyrins due to deficiencies in enzymes involved in hemoglobin
532 metabolism(68). How exactly tissue damage and photosensitivity occur in porphyria is currently
533 not understood. Intriguingly, it was shown that ROS accumulate in porphyria and surprisingly,
534 certain porphyrins can stabilize Z-DNA(69). This raises the question whether cutaneous Z-DNA
535 might be involved in the entire spectrum of photosensitivity, not just those promoted by
536 autoimmune diseases.

537 Together, our results uncover a new mechanism of autoimmune photosensitivity driving innate
538 immune responses in the skin of lupus and DM patients that could be important for other
539 photosensitive skin diseases. Both Z-DNA and ZBP1 represent new cutaneous targets for the
540 prevention and potential treatment of lupus and DM skin disease.

541

542

543 **Methods:**

544 **Human Subjects**

545 All human subject protocols were reviewed and approved by the University of Michigan IRB-
546 Med. Skin samples from patients with SLE with a history of cutaneous lupus and sex and age-
547 matched healthy controls were obtained with written, informed consent according to the
548 Declaration of Helsinki.

549 **Cell culture**

550 Immortalized N/TERT keratinocytes (N/TERT-2G) (41), were used with permission from James
551 G. Rheinwald (Brigham and Women's Hospital, Boston, Massachusetts, USA). N/TERTs were
552 grown in Keratinocyte-SFM medium (ThermoFisher #17005-042) supplemented with 30 µg/ml
553 bovine pituitary extract, 0.2 ng/ml epidermal growth factor, and 0.3 mM calcium chloride.
554 N/TERTs were used from passage 6 to passage 20. Primary human keratinocytes from SLE
555 patients and age and sex matched controls were isolated from non-lesional, non-sun-exposed
556 skin as previously described(13) and used at passages 2-6 and grown in Epilife medium (Gibco,
557 #MEPI500CA) with added human keratinocyte growth supplement (10ul/ml medium).
558 Demographics and clinical characteristics of patients and controls used for cell culture are
559 shown in Supplemental Table 1.

560 STING KO keratinocytes were generated as previously described(70). N/TERTs overexpressing
561 *ZBP1* were generated as follows: Full length human Z-DNA binding protein 1 (ZBP1) cDNA,
562 transcript variant 1, was obtained from GenScript (OHu21369). PCR was performed to add the
563 3XFlag tag to the N terminus of ZBP1 cDNA at the 5' Not1 site and 3' Sal1 site to facilitate
564 cloning into expressing vector p3XFlag-CMV-7.1 (Sigma). The resulting plasmid containing the
565 3XFlag-ZBP1 was further subcloned in the Bst1 and BamHI sites of the vector pLVX-EF1α-
566 AcGFP1-C1 (Takara, cat# 631984, simplified as pLvX-GFP) by PCR to generate the lentivirus
567 overexpressing vector pLVX-GFP-3XFlag-ZBP1 (simplified as pLvX-GFP-ZBP1OE). The
568 constructs were confirmed by sequencing. For Lentiviral infection, the lentiviral empty vector
569 pLvX-GFP and overexpressing pLvX-GFP-ZBP1OE were transiently transfected to 293T cells
570 with packaging plasmids pxPAX2 and pMD2 by the Lipofectamine 2000 to produce the lentivirus
571 as described previously (Bin Xu Plos One 2010). The supernatant containing the lentivirus was
572 used to infect the N/TERTs followed by puromycin selection at 10ug/mL.

573 Knockdown of ZBP1 in N/TERTs was performed using a lentivirus expressing either shRNA
574 targeting Human ZBP1 or shcontrol. Two different Mission lentivirus-based plasmids of shRNAs

575 (clone numbers TRCN0000123050 and TRCN0000436778) against human ZBP1 and the
576 shcontrol vector TRC2 pLKO.5-puro nonmammalian shRNA (SHC202) were obtained from
577 Sigma-Aldrich (Burlington, MA). 293T cells were cotransfected with the shRNA and packaging
578 plasmids psPAX2 and pMD2 using Lipofectamine 2000 (Invitrogen) in OptiMEM (Gibco) for 6
579 hrs followed by replacing with keratinocyte medium to produce the lentivirus. Twenty-four hours
580 post transfection, the virus-containing media was collected and centrifuged for 5min at 2000 rpm
581 at 4° C. The resulting supernatant was supplemented with 8 µg/ml Polybrene (Sigma) and used
582 to infect the sub-confluent N/TERTs. The 293T cells were replaced with fresh keratinocyte
583 media and were subsequently used to repeat the N/TERT cell infection two additional times at
584 intervals of 8 to 12 h. N/TERTs infected with either shRNA or shcontrol were selected at 10-
585 12ug/ml puromycin and cells were maintained in 10ug/ml puromycin until the day of experiment.

586 **UV irradiation**

587 Keratinocytes were grown on either 6 well plates on uncoated glass slides (ThermoScientific,
588 22x22mm, #3406) for microscopy or 12 well plates for analysis of gene expression. On the day
589 of UVB irradiation, media was changed to prewarmed PBS and cells were irradiated with a dose
590 of 50mJ/cm² using the UV-2 ultraviolet irradiation system (Tyler Research). Emission of UVB
591 radiation (310nm) was allowed by cascade-phosphor ultraviolet generators. Immediately after
592 irradiation, fresh prewarmed media was added until further analysis.

593

594 **mitoTEMPO treatment**

595 To reduce mtROS, cells were incubated with mitoTEMPO (Sigma Aldrich, SML0737) (50µM in
596 DMSO) or DMSO 0.5% alone as a control 45min prior to UVB exposure in Keratinocyte SFM.
597 After UVB exposure, fresh mitoTEMPO and medium was added to the wells until further
598 analysis. No differences in mitoSOX staining, confocal microscopy or gene expression were
599 observed with phenol-red containing Keratinocyte SFM vs. phenol-red free media, hence
600 phenol-red containing Keratinocyte SFM was used. Rotenone was used as a positive control for
601 mitoROS (0.5µM).

602

603 **Analysis of mitochondrial superoxide (mitoSOX) staining**

604 Keratinocytes were first plated on glass-bottom (no. 1.5) 96-well Mat-Tek dishes and grew for
605 36h. Cells were then pretreated with mitoTEMPO 45min prior to UVB exposure and then
606 irradiated in PBS (see mitoTEMPO treatment and UV irradiation) and incubated for 30min.
607 Within the last 20 min of the experiment, cells were stained with 2.5µM MitoSOX red dye

608 (Thermo Fisher Scientific, M36008) and Hoechst33342 (1 $\mu\text{g/ml}$) for 20 min at 37°C, protected
609 from light. Then, cells were washed with PBS and fixed with 4% PFA at RT for 15 min. Lastly,
610 cells were washed with PBS and then immediately imaged using a Nikon Yokogawa X1-CSU
611 spinning disk confocal microscope. Fields of view were selected based on the Hoechst stain.

612

613 **RNA isolation, cDNA synthesis and qtPCR**

614 For RNA isolation, the Qiagen RNeasy Plus Mini kit was used according to the manufacturer's
615 instructions. After isolation of RNA, samples were diluted in 20-40ul RNase free water,
616 depending on target RNA concentrations desired. Total RNA quantification and RNA purity were
617 determined based on the ratio A260nm/A280 nm using Thermo Fisher Scientific NANO drop
618 2000. A total of 500 to 1000ng of cDNA was synthesized using the iScript cDNA synthesis kit
619 (BioRad, #1708891). 10ng cDNA was used for quantitative PCR in technical triplicates in a 384
620 well plate using SYBR Green Supermix (Applied Biosystems). PCR was run in Applied
621 Biosystems QuantStudio™ 12K Flex Real-Time PCR at the Advanced Genomics Core at the
622 University of Michigan. Primer sequences are summarized in Supplemental Table 4. Gene
623 expression level was determined by relating to the housekeeper gene beta-Actin or RPLP0
624 using the $\Delta\Delta\text{ct}$ method setting the mock condition to one.

625

626 **Immunofluorescence staining cell culture**

627 Keratinocytes were plated on coverslips in a 6 well plate. Mitochondrial ROS were stained
628 30min after UVB exposure. 8oxodG, Z-DNA and mitochondrial dynamics were stained 3h after
629 UVB exposure. At each experimental endpoint, cells were fixed with freshly prepared 4%
630 paraformaldehyde (PFA) at RT for 15min. The IFA was always performed on the same day as
631 the experiment. After fixation, cells were washed with PBS + 0.1% TritonX100 (wash buffer) and
632 then blocked with 5% BSA and 10% normal goat serum in wash buffer (block buffer) for 30min
633 at RT. Primary antibody cocktails were prepared in block buffer and incubated on each coverslip
634 for 1h at RT. Then, wells were washed three times using wash buffer and incubated with
635 secondary antibodies and counterstains diluted in block buffer for 30min at RT. After this, wells
636 were washed three times using wash buffer and coverslips were mounted on glass slides using
637 ProLong Glass Antifade Mountant (Invitrogen, P36980). Large (3x3) images were taken the next
638 day either with 60X or 100X magnification, depending on the staining, on a Nikon Yokogawa
639 spinning disk microscope. Using large image acquisition, over 250 - 500 cells per condition
640 could be stained. Specific antibody details are available in Supplemental Table 3. Operator bias

641 was reduced during image acquisition through selection of fields of view and focal planes based
642 on counterstains that were unrelated to the experimental question (DAPI or CellTracker).

643

644 **Intensity Line Measurement**

645 Representative images for intensity measurement were taken on a Nikon Yokogawa spinning
646 disk microscope and pixel intensity was assessed with Fiji (ImageJ) to measure indicated
647 staining (TOMM20, Z-DNA and 8oxodG) intensity across the dotted lines at baseline and after
648 UVB exposure.

649

650 **Automatic image analysis**

651 Confocal microscopy images were quantified by automated image analysis using CellProfiler,
652 an open-source software. All CellProfiler pipelines associated with this work are available in
653 supplemental files (Supplemental file 1). Analysis of images was performed on raw images
654 unless otherwise specified. Briefly, single-cells were identified by nuclear objects based on
655 global thresholding of nuclear staining (DAPI, 4',6-diamidino-2-phenylindole or Hoechst) using
656 the “identify primary objects” module, followed by propagation of the nuclear objects to the
657 cellular periphery based on a whole-cell stain (CellTracker) using the identify secondary objects
658 module. Subsequently, a variety of cellular parameters were measured and related to parent
659 cells using the relate objects module.

660 For the quantification of mitochondrial superoxide (Supplemental file 1, Figure 1 C), the intensity
661 of the mitochondrial superoxide indicator MitoSOX was analyzed within cells using Hoechst as
662 the nuclear counterstain and defining cells by propagation of the nuclear objects to the cellular
663 periphery based on mitoSOX staining.

664 Mitochondria were determined using the TOMM20 immunostaining with two-class Otsu adaptive
665 thresholding within the “identify primary objects” module, and the mitochondrial compartment
666 was determined by using the “merge objects” to connect adjacent mitochondrial objects
667 (neighbor distance 0 pixels). To measure Z-DNA puncta outside of the mitochondrial
668 compartment (Supplemental file 1, Figure 1L), puncta in the Z-DNA immunostaining were
669 identified using the primary objects module. The cytosolic mitochondria-free content was
670 created using the “identify tertiary objects” module by defining the non-nuclear compartment as
671 the CellTracker-positive and DAPI-negative space and subsequently the cytosol by subtracting
672 the mitochondrial staining (by TOMM20) from the non-nuclear compartment to get the

673 mitochondria-free cytosolic compartment. Tertiary objects were then related to cells by using the
674 “relate objects” module to determine cytosolic Z-DNA puncta per cell.

675 For analysis of 8-Oxo-2'-desoxyguanosine (8oxodG, Supplemental file 1, Fig. 2, A and D), the
676 intensity of the 8oxodG staining was analyzed within cell objects (defined as ‘total’ in the
677 manuscript) as well as within the mitochondrial compartment which was defined by
678 segmentation of mitochondrial staining (anti-TOMM20). For the correlation of 8oxodG with total
679 and cytosolic Z-DNA (Figure 2D), intensity values of 8oxodG per cell and Z-DNA puncta per cell
680 across all images and different conditions were matched and the average intensity of 8oxodG
681 for the counts of Z-DNA puncta was calculated. The corresponding intensity to Z-DNA puncta
682 counts were then plotted and correlated using Pearson correlation analysis. For correlation of
683 mitochondrial fragments with total and cytosolic Z-DNA, mitochondrial fragments per cell were
684 calculated, plotted against Z-DNA puncta counts per cell and then correlated using Pearson
685 correlation analysis.

686 In Figure 4F, intensity values for epidermal ZBP1 were determined using manual identification
687 of the epidermis based on nuclear staining of slides with DAPI. Average intensity per image with
688 similar epidermal areas including >300 cells were included in the analysis.

689 In Figure 6G, cGAS intensity per cell was quantified within nuclear objects, and the total
690 cytoplasm (nuclear subtracted cellular area, based on GFP). The nuclear:cytoplasmic ratio
691 was calculated by dividing nuclear and cytoplasmic intensity for each cell.

692 Removal of outliers resulting from automated image analysis was performed using strict ROUT
693 outlier identification ($Q = 0.1\%$) in GraphPad Prism from cell-level data pooled across multiple
694 experiments. Representative confocal images shown in this manuscript were prepared using the
695 ImageJ background subtraction tool with a rolling ball radius of 30 pixels. Operator bias during
696 image acquisition was reduced by selecting fields of view and cells based on counterstains that
697 were unrelated to the staining of primary interest.

698

699 **Depletion of mtDNA using ddC**

700 To reduce total mtDNA content, we treated N/TERTs with 2'-3'-dideoxycytidine (ddC) according
701 to a previously published protocol(71) with the following modifications: N/TERTs were seeded in
702 a 6 well plate at 15-20% confluency and 12h after seeding medium was changed containing
703 ddC (50 μ M and 150 μ M). Medium was changed every 24h until confluency reached 70-80%

704 after 2 days. Then, cells were irradiated with UVB exposure (see above). Z-DNA staining was
705 assessed 3h after UVB exposure and gene expression was assessed 6h after irradiation.

706

707 **Cellular ROS measurement**

708 For detection of cellular ROS, we used the indicator CM-H₂DCFDA (Invitrogen) and cells were
709 incubated with CM-H₂DCFDA 10uM for 30 minutes prior to UVB exposure. Phenol red-free
710 keratinocyte media (Gibco) was added, and fluorescence was measured five minutes post UVB
711 exposure using a microplate reader (Ex/Em 492/527 nm). The average of 3-5 replicates per
712 condition were averaged in each experiment (n=4-6), background fluorescence was subtracted,
713 and data was expressed as fold change relative to untreated.

714

715 **Measurement of B-DNA and Z-DNA conformation using ratio of A260/295**

716 Conformation of Z-DNA and B-DNA was assessed using the absorbance ratio of 260 to 295nm
717 as previously described(43, 45). We used poly(dGdC) (50ng/μl) for conformation analysis.
718 Poly(dGdC) was diluted in water with increasing salt concentrations (titration of 1.8M, 2M, 2.2M,
719 2.4M, 2.6M, 2.8M, 3M, 3.2M, 3.4M, 3.6M and 4M NaCl) to induce Z-DNA conformation.
720 Reaction was performed for 2h at 37°C in nuclease-free microcentrifuge tubes (BioRad).
721 A260/295 was measured with a nanodrop (company) using water with different salt
722 concentrations as a blank. For induction of Z-DNA by H₂O₂, poly(dGdC) was diluted in water
723 containing 1mM H₂O₂ and increasing salt concentrations as mentioned above. Samples were
724 incubated for 2h at 37°C and were measured with a nanodrop using 1mM H₂O₂ with different
725 salt concentrations (absent DNA) as blanks. Each incubation was performed in triplicates. The
726 values were then plotted as the ratio of A260/295.

727

728 **Skin genome-wide expression datasets**

729 Three previously published microarray datasets were used for analysis. These included
730 samples from: 1. healthy controls (n=13) and lesional skin of patients with lupus (n=90, of these
731 47 DLE and 43 SCLE)(72); 2. healthy controls (n=5) and dermatomyositis (n=41 biopsies from
732 36 patients)(16); and 3. healthy pediatric controls (n=8) and childhood onset systemic lupus
733 (n=7 lesional skin biopsies from 5 patients) and juvenile dermatomyositis (n=9 lesional skin
734 biopsies from 9 patients)(73). Microarray datasets are available from CLE through GEO
735 GSE81071, from adult DM through GSE142807, from childhood SLE and juvenile DM through
736 GEO GSE148810. As we previously published, Pearson correlation analysis was performed

737 between gene expression and a previously described 6 IFN-stimulated gene score(73, 74) using
738 GraphPad Prism version 9.1.0.

739

740 **Single cell Sequencing**

741 For Fig. 3, F, expression of *ZBP1* was examined from our single cell RNA sequencing dataset in
742 nonlesional (n=14), lesional (n=14) and healthy control (n=14) skin(12). Specifically, *ZBP1*
743 expression was plotted across the major cell types defined in the single cell RNA sequencing
744 dataset, and these cell types were further divided by the disease states of the cells.

745

746 **Tissue immunofluorescence**

747 To assess tissue protein expression, formalin-fixed, paraffin-embedded tissue slides were
748 obtained from patients with cutaneous lupus (chronic discoid lupus, subacute cutaneous lupus
749 and nonlesional skin from systemic lupus patients), dermatomyositis (lesional and nonlesional
750 skin) and healthy controls. Slides were heated for 1h at 60°C, rehydrated, and antigen retrieved
751 with tris-EDTA (pH6). Slides were blocked with blocking buffer (PBS + 10% normal goat serum)
752 and then incubated with primary antibodies (diluted in blocking buffer) against *ZBP1*
753 (Supplemental Table 3) overnight at 4°C. Slides were incubated with secondary antibodies
754 (Supplemental Table 3) and counterstained with 4',6-diamidino-2-phenylindole (DAPI). Slides
755 were mounted with Antifade glass mounting medium (ThermoFisher) and dried overnight at
756 room temperature in the dark. Images were acquired using a Zeiss Axioskop 2 microscope and
757 analyzed using CellProfiler (see above). Images presented are representative of at least five
758 biologic replicates. Patient characteristics for samples from SCLE/DLE and DM patients are
759 shown in Supplemental Table 2. Controls were anonymized biopsies from healthy control
760 without history of skin disease.

761

762 **DNA transfection**

763 Primary control keratinocytes or N/TERTs were seeded in triplicates in a 12 well plate and
764 grown for 48h in appropriate media to 60-70% confluence (see above). DNA transfection was
765 performed using Lipofectamine2000 and diluted dsDNA (50ng/μl, B-DNA equivalent) as well as
766 polydGdC (50ng/μl, Z-DNA equivalent). After warming all reagents and media up to RT,
767 Lipofectamine2000 (11668-029) and DNA were diluted in OptiMEM (Gibco, #31985-070) at a
768 ratio of 3μl/μg DNA. Cells were covered with 400μl of OptiMEM containing either 50ng DNA
769 (125ng DNA/ml media) or 100ng DNA (250ng DNA/ml media) and incubated at 37C until further

770 analysis. 4h after transfection, cells were washed with ice-cold PBS and then lysed for phospho-
771 Western Blot with Protease inhibitor (cOmplete Mini, EDTA-free, Sigma, #11836170001) and
772 Phosphatase Inhibitor Cocktail (Pierce, PI78420). 6h and 24h after transfection, cells were
773 analyzed for gene expression using the Qiagen RNeasy Plus Mini Kit and qtPCR (see above).

774

775 **Western Blot**

776 Cells were washed with ice-cold PBS and then lysed. Prior to sodium dodecyl sulfate-
777 polyacrylamide gel electrophoresis (SDS-PAGE), sample protein content was normalized by
778 dilution following a Bradford assay. Samples were diluted in Laemmli sample loading buffer
779 supplemented with β -mercaptoethanol (Bio-Rad), heated for 5 min at 95°C, and then separated
780 on 4 to 20% gradient polyacrylamide tris-glycine gels (Bio-Rad). After SDS-PAGE, gels were
781 transferred to a 0.45- μ m nitrocellulose membrane by a semi-dry transfer system (Cytiva) and
782 membranes were blocked with PBS + 5% BSA + 0.1% Tween20 (blocking buffer) for 30min at
783 room temperature on a shaker. After blocking, primary antibodies were diluted in blocking buffer
784 and added to incubated overnight at 4°C on a shaker. Secondary antibodies diluted in blocking
785 buffer were added and incubated for 30min at room temperature in the dark. Image acquisition
786 was accomplished using LI-COR IR dye secondary antibodies and an Odyssey IR Imager.
787 Quantification of Western blots was performed using ImageJ densitometric gel analysis for 1D
788 gels. Antibodies and dilutions for Western Blot are listed in Supplemental Table 3.

789

790

791 **References:**

792

- 793 1. J. Wenzel, Cutaneous lupus erythematosus: new insights into pathogenesis and therapeutic
794 strategies. *Nature Reviews Rheumatology* **15**, 519-532 (2019).
- 795 2. S. N. Estadt, M. P. Maz, J. Musai, J. M. Kahlenberg, Mechanisms of Photosensitivity in
796 Autoimmunity. *J Invest Dermatol* **142**, 849-856 (2022).
- 797 3. M. K. Sarkar *et al.*, Photosensitivity and type I IFN responses in cutaneous lupus are driven by
798 epidermal-derived interferon kappa. *Ann Rheum Dis* **77**, 1653-1664 (2018).
- 799 4. J. H. Sim *et al.*, Immune Cell–Stromal Circuitry in Lupus Photosensitivity. *The Journal of*
800 *Immunology* **206**, 302-309 (2021).
- 801 5. K. Foering *et al.*, Characterization of clinical photosensitivity in cutaneous lupus erythematosus.
802 *Journal of the American Academy of Dermatology* **69**, 205-213 (2013).
- 803 6. M. P. Maz *et al.*, Recent advances in cutaneous lupus. *Journal of autoimmunity* **132**, 102865
804 (2022).
- 805 7. S. Skopelja-Gardner *et al.*, Acute skin exposure to ultraviolet light triggers neutrophil-mediated
806 kidney inflammation. **118**, e2019097118 (2021).
- 807 8. K. L. Clark *et al.*, Epidermal injury promotes nephritis flare in lupus-prone mice. *Journal of*
808 *autoimmunity* **65**, 38-48 (2015).
- 809 9. E. L. Gutmark, D. Q. Lin, I. Bernstein, S. Q. Wang, B. F. Chong, Sunscreen use in patients with
810 cutaneous lupus erythematosus. *The British journal of dermatology* **173**, 831-834 (2015).
- 811 10. A. Psarras *et al.*, Functionally impaired plasmacytoid dendritic cells and non-haematopoietic
812 sources of type I interferon characterize human autoimmunity. *Nature Communications* **11**, 6149
813 (2020).
- 814 11. A. Psarras, M. Wittmann, E. M. Vital, Emerging concepts of type I interferons in SLE
815 pathogenesis and therapy. *Nat Rev Rheumatol* **18**, 575-590 (2022).
- 816 12. A. C. Billi *et al.*, Nonlesional lupus skin contributes to inflammatory education of myeloid cells and
817 primes for cutaneous inflammation. **14**, eabn2263 (2022).
- 818 13. J. N. Stannard *et al.*, Lupus Skin Is Primed for IL-6 Inflammatory Responses through a
819 Keratinocyte-Mediated Autocrine Type I Interferon Loop. *J Invest Dermatol* **137**, 115-122 (2017).
- 820 14. L. C. Tsoi *et al.*, Hypersensitive IFN Responses in Lupus Keratinocytes Reveal Key Mechanistic
821 Determinants in Cutaneous Lupus. *J Immunol* **202**, 2121-2130 (2019).
- 822 15. M. M. Tabata *et al.*, The Type I Interferon Signature Reflects Multiple Phenotypic and Activity
823 Measures in Dermatomyositis. **n/a**.
- 824 16. L. C. Tsoi *et al.*, IL18-containing 5-gene signature distinguishes histologically identical
825 dermatomyositis and lupus erythematosus skin lesions. *JCI Insight* **5**, (2021).
- 826 17. R. R. Goel, S. V. Kotenko, M. J. Kaplan, Interferon lambda in inflammation and autoimmune
827 rheumatic diseases. *Nat Rev Rheumatol* **17**, 349-362 (2021).

- 828 18. S. Zahn *et al.*, Evidence for a Pathophysiological Role of Keratinocyte-Derived Type III Interferon
829 (IFN λ) in Cutaneous Lupus Erythematosus. *Journal of Investigative Dermatology* **131**, 133-140
830 (2011).
- 831 19. M. A. Birch-Machin, E. V. Russell, J. A. Latimer, Mitochondrial DNA damage as a biomarker for
832 ultraviolet radiation exposure and oxidative stress. *British Journal of Dermatology* **169**, 9-14
833 (2013).
- 834 20. R. Jugé *et al.*, Quantification and Characterization of UVB-Induced Mitochondrial Fragmentation
835 in Normal Primary Human Keratinocytes. *Scientific Reports* **6**, 35065 (2016).
- 836 21. C. Li *et al.*, Impaired mitophagy causes mitochondrial DNA leakage and STING activation in
837 ultraviolet B-irradiated human keratinocytes HaCaT. *Archives of Biochemistry and Biophysics*
838 **737**, 109553 (2023).
- 839 22. I. Golovynska, S. Golovynskyi, J. Qu, Comparing the Impact of NIR, Visible and UV Light on ROS
840 Upregulation via Photoacceptors of Mitochondrial Complexes in Normal, Immune and Cancer
841 Cells. **99**, 106-119 (2023).
- 842 23. N. Gehrke *et al.*, Oxidative damage of DNA confers resistance to cytosolic nuclease TREX1
843 degradation and potentiates STING-dependent immune sensing. *Immunity* **39**, 482-495 (2013).
- 844 24. S. Skopelja-Gardner *et al.*, The early local and systemic Type I interferon responses to ultraviolet
845 B light exposure are cGAS dependent. *Scientific Reports* **10**, 7908 (2020).
- 846 25. N. Berndt *et al.*, Photosensitivity and cGAS-Dependent IFN-1 Activation in Patients with Lupus
847 and TREX1 Deficiency. *Journal of Investigative Dermatology* **142**, 633-640.e636 (2022).
- 848 26. J. S. Riley, S. W. Tait, Mitochondrial DNA in inflammation and immunity. *EMBO reports* **21**,
849 e49799 (2020).
- 850 27. A. P. West, G. S. Shadel, Mitochondrial DNA in innate immune responses and inflammatory
851 pathology. *Nature Reviews Immunology* **17**, 363-375 (2017).
- 852 28. C. Lood *et al.*, Neutrophil extracellular traps enriched in oxidized mitochondrial DNA are
853 interferogenic and contribute to lupus-like disease. *Nat Med* **22**, 146-153 (2016).
- 854 29. S. Caielli *et al.*, Oxidized mitochondrial nucleoids released by neutrophils drive type I interferon
855 production in human lupus. *Journal of Experimental Medicine* **213**, 697-713 (2016).
- 856 30. N. Miao *et al.*, Oxidized mitochondrial DNA induces gasdermin D oligomerization in systemic
857 lupus erythematosus. *Nat Commun* **14**, 872 (2023).
- 858 31. S. Caielli *et al.*, Erythroid mitochondrial retention triggers myeloid-dependent type I interferon in
859 human SLE. *Cell* **184**, 4464-4479.e4419 (2021).
- 860 32. L. E. Newman, G. S. Shadel, Mitochondrial DNA Release in Innate Immune Signaling. *Annu Rev*
861 *Biochem* **92**, 299-332 (2023).
- 862 33. A. P. West *et al.*, Mitochondrial DNA stress primes the antiviral innate immune response. *Nature*
863 **520**, 553-557 (2015).

- 864 34. Y. Lei *et al.*, Cooperative sensing of mitochondrial DNA by ZBP1 and cGAS promotes
865 cardiotoxicity. *Cell*, (2023).
- 866 35. J. Maelfait, J. Rehwinkel, The Z-nucleic acid sensor ZBP1 in health and disease. *Journal of*
867 *Experimental Medicine* **220**, (2023).
- 868 36. A. Takaoka *et al.*, DAI (DLM-1/ZBP1) is a cytosolic DNA sensor and an activator of innate
869 immune response. *Nature* **448**, 501-505 (2007).
- 870 37. N. W. Hubbard *et al.*, ADAR1 mutation causes ZBP1-dependent immunopathology. *Nature* **607**,
871 769-775 (2022).
- 872 38. A. Herbert, Z-DNA and Z-RNA in human disease. *Commun Biol* **2**, 7 (2019).
- 873 39. H. Jiao *et al.*, Z-nucleic-acid sensing triggers ZBP1-dependent necroptosis and inflammation.
874 *Nature* **580**, 391-395 (2020).
- 875 40. J. Wang, S. Wang, C. Zhong, T. Tian, X. Zhou, Novel insights into a major DNA oxidative lesion:
876 its effects on Z-DNA stabilization. *Organic & Biomolecular Chemistry* **13**, 8996-8999 (2015).
- 877 41. J. Saada *et al.*, Oxidative stress induces Z-DNA-binding protein 1-dependent activation of
878 microglia via mtDNA released from retinal pigment epithelial cells. *J Biol Chem* **298**, 101523
879 (2022).
- 880 42. N. Li *et al.*, Mitochondrial complex I inhibitor rotenone induces apoptosis through enhancing
881 mitochondrial reactive oxygen species production. **278**, 8516-8525 (2003).
- 882 43. J. B. Chaires, Allosteric conversion of Z DNA to an intercalated right-handed conformation by
883 daunomycin. *Journal of Biological Chemistry* **261**, 8899-8907 (1986).
- 884 44. F. M. Pohl, T. M. Jovin, Salt-induced co-operative conformational change of a synthetic DNA:
885 Equilibrium and kinetic studies with poly(dG-dC). *Journal of Molecular Biology* **67**, 375-396
886 (1972).
- 887 45. J. R. Buzzo *et al.*, Z-form extracellular DNA is a structural component of the bacterial biofilm
888 matrix. *Cell* **184**, 5740-5758.e5717 (2021).
- 889 46. T. J. Thomas, U. B. Gunnia, T. Thomas, Polyamine-induced B-DNA to Z-DNA conformational
890 transition of a plasmid DNA with (dG-dC)_n insert. *Journal of Biological Chemistry* **266**, 6137-6141
891 (1991).
- 892 47. J. Kim *et al.*, VDAC oligomers form mitochondrial pores to release mtDNA fragments and
893 promote lupus-like disease. *Science (New York, N. Y.)* **366**, 1531-1536 (2019).
- 894 48. S. Victorelli *et al.*, Apoptotic stress causes mtDNA release during senescence and drives the
895 SASP. *Nature* **622**, 627-636 (2023).
- 896 49. Y. Huang, D. D. Yang, X. Y. Li, D. L. Fang, W. J. Zhou, ZBP1 is a significant pyroptosis regulator
897 for systemic lupus erythematosus. *Annals of translational medicine* **9**, 1773 (2021).
- 898 50. S. Caielli, Z. Wan, V. Pascual, Systemic Lupus Erythematosus Pathogenesis: Interferon and
899 Beyond. *Annu Rev Immunol*, (2023).

- 900 51. D. M. Spencer, E. Svenungsson, I. Gunnarsson, R. Caricchio, D. S. Pisetsky, The expression of
901 antibodies to Z-DNA in the blood of patients with systemic lupus erythematosus: Relationship to
902 autoantibodies to B-DNA. *Clinical immunology (Orlando, Fla.)* **255**, 109763 (2023).
- 903 52. E. M. Lafer *et al.*, Z-DNA-specific antibodies in human systemic lupus erythematosus. *The*
904 *Journal of clinical investigation* **71**, 314-321 (1983).
- 905 53. E. Erdal, S. Haider, J. Rehwinkel, A. L. Harris, P. J. McHugh, A pro-survival DNA damage-induced
906 cytoplasmic interferon response is mediated by end resection factors and is limited by Trex1.
907 *Genes & development* **31**, 353-369 (2017).
- 908 54. C. Wolf *et al.*, RPA and Rad51 constitute a cell intrinsic mechanism to protect the cytosol from
909 self DNA. *Nature Communications* **7**, 11752 (2016).
- 910 55. S. Glück *et al.*, Innate immune sensing of cytosolic chromatin fragments through cGAS promotes
911 senescence. *Nat Cell Biol* **19**, 1061-1070 (2017).
- 912 56. M. Gratia *et al.*, Bloom syndrome protein restrains innate immune sensing of micronuclei by
913 cGAS. *J Exp Med* **216**, 1199-1213 (2019).
- 914 57. Q. Yu *et al.*, DNA-damage-induced type I interferon promotes senescence and inhibits stem cell
915 function. *Cell Rep* **11**, 785-797 (2015).
- 916 58. A. G. Singh *et al.*, Cancer risk in cutaneous lupus erythematosus: a population-based cohort
917 study. *Rheumatology* **55**, 2009-2013 (2016).
- 918 59. M. A. Sherwani *et al.*, Type I Interferons Enhance the Repair of Ultraviolet Radiation-Induced
919 DNA Damage and Regulate Cutaneous Immune Suppression. *International journal of molecular*
920 *sciences* **23**, (2022).
- 921 60. H. He *et al.*, Role of mitochondria on UV-induced skin damage and molecular mechanisms of
922 active chemical compounds targeting mitochondria. *Journal of Photochemistry and Photobiology*
923 *B: Biology* **232**, 112464 (2022).
- 924 61. K. J. Mackenzie *et al.*, cGAS surveillance of micronuclei links genome instability to innate
925 immunity. *Nature* **548**, 461-465 (2017).
- 926 62. H. Jiao *et al.*, ADAR1 averts fatal type I interferon induction by ZBP1. *Nature* **607**, 776-783
927 (2022).
- 928 63. T. Zhang *et al.*, ADAR1 masks the cancer immunotherapeutic promise of ZBP1-driven
929 necroptosis. *Nature* **606**, 594-602 (2022).
- 930 64. R. de Reuver *et al.*, ADAR1 prevents autoinflammation by suppressing spontaneous ZBP1
931 activation. *Nature* **607**, 784-789 (2022).
- 932 65. M. Devos *et al.*, Sensing of endogenous nucleic acids by ZBP1 induces keratinocyte necroptosis
933 and skin inflammation. *J Exp Med* **217**, (2020).
- 934 66. L. Freund *et al.*, IFN γ Causes Keratinocyte Necroptosis in Acute Graft-Versus-Host Disease. *J*
935 *Invest Dermatol* **143**, 1746-1756.e1749 (2023).

- 936 67. S. Lee *et al.*, AIM2 forms a complex with pyrin and ZBP1 to drive PANoptosis and host defence.
937 *Nature* **597**, 415-419 (2021).
- 938 68. D. M. Bissell, K. E. Anderson, H. L. Bonkovsky, Porphyria. **377**, 862-872 (2017).
- 939 69. A. D'Urso *et al.*, Interactions of a Tetraanionic Porphyrin with DNA: from a Z-DNA Sensor to a
940 Versatile Supramolecular Device. *Journal of the American Chemical Society* **131**, 2046-2047
941 (2009).
- 942 70. M. K. Sarkar *et al.*, Keratinocytes sense and eliminate CRISPR DNA through STING/IFN- κ
943 activation and APOBEC3G induction. *The Journal of clinical investigation* **133**, (2023).
- 944 71. J. D. Bryant, Y. Lei, J. J. VanPortfliet, A. D. Winters, A. P. West, Assessing Mitochondrial DNA
945 Release into the Cytosol and Subsequent Activation of Innate Immune-related Pathways in
946 Mammalian Cells. *Curr Protoc* **2**, e372 (2022).
- 947 72. C. C. Berthier *et al.*, Molecular Profiling of Cutaneous Lupus Lesions Identifies Subgroups Distinct
948 from Clinical Phenotypes. *J Clin Med* **8**, (2019).
- 949 73. J. L. Turnier *et al.*, Comparison of Lesional Juvenile Myositis and Lupus Skin Reveals
950 Overlapping Yet Unique Disease Pathophysiology. *Arthritis & rheumatology (Hoboken, N.J.)* **73**,
951 1062-1072 (2021).
- 952 74. X. Feng *et al.*, Association of increased interferon-inducible gene expression with disease activity
953 and lupus nephritis in patients with systemic lupus erythematosus. **54**, 2951-2962 (2006).
954

955 **Acknowledgements:**

956 We thank the patients for participation in this study. We thank Chrissy Goudsmit and Sri
957 Yalavarthi for helpful technical assistance. We acknowledge the assistance of the Microscopy
958 core and the Advanced Genomics core at the University of Michigan.

959

960 **Funding:**

961 This work was supported by the National Institutes of Health through awards R01AR071384,
962 K24AR076975, R03AR066337 (JMK), P30AR075043 (JEG), R01AI157384 (MOR),
963 K23AR080789 (JLT), German Research Foundation fund KL3612/1-1 (BK), Rheumatology
964 Research Foundation Investigator Award 025850 (JLT), Cure JM Award Michigan12/20 (JLT),
965 University of Michigan Immunology Program Research Training in Experimental Immunology
966 training grant T32 AI007413 (MR), Miller Fund Award for Innovative Immunology Research
967 (MR), American Heart Association and Barth Syndrome Foundation co-funded predoctoral
968 fellowship 23PRE1019408 (MR), the George M. O'Brien Michigan Kidney Translational
969 Research Core Center P30DK081943 (CB) and the Taubman Institute Innovative Programs
970 (JMK and JEG).

971

972 **Author contributions:**

973 Conceptualization: BK, MK; Methodology: BK, MR, BX, MGK, CB, SH, SE, JEG, KEM, AV, CD,
974 MOR, JMK; Investigation: BK, MR, BX, MGK, YG, CB, AV, SE, SH, CD, GH, FM, JT, JEG,
975 MOR, JMK; funding acquisition: BK, MR, MOR, MK; Visualization: BK, MR, BX, MGK, CB, SH;
976 project administration: MK; Supervision: JEG, MOR, JMK; writing-original draft: BK, KM; writing
977 – review and editing: BK, MR, JT, JEG, MOR, JMK

978

979 **Competing interests:**

980 JMK has received grant support from Q32 Bio, Celgene/Bristol-Myers Squibb, Ventus
981 Therapeutics, Rome Therapeutics, and Janssen. JMK has served on advisory boards for
982 AstraZeneca, Bristol-Myers Squibb, Eli Lilly, EMD serrano, Gilead, GlaxoSmithKline, Aurinia
983 Pharmaceuticals, Rome Therapeutics, and Ventus Therapeutics. JEG has received support
984 from Eli Lilly, Janssen, BMS, Sanofi, Prometheus, Almirall, Kyowa-Kirin, Novartis, AnaptysBio,
985 Boehringer Ingelheim, Regeneron, AbbVie, and Galderma.

986

987 **Data and materials availability:**

988 Skin wide genome expression datasets are already available for CLE through GEO GSE81071,
989 from adult DM through GSE142807, from childhood SLE and juvenile DM through GEO GSE14
990 8810. The scRNA-seq data are available in GEO under accession number GSE186476.
991 Pipelines for automated image analysis in Cell Profiler are within the Supplemental files of this
992 manuscript. All other data supporting the conclusions of the manuscript including patient data
993 are available in the main text or the supplemental figures and tables.
994

995 **Supplemental Materials:**

996 **Figs. S1 to S9:**

997 Supplemental Figure 1. UVB-driven IFN responses are mtDNA dependent and UV-induced Z-
998 DNA derives from mtDNA.

999 Supplemental Figure 2. UVB induces oxidative DNA damage in the cytosol and mitochondrial
1000 compartment.

1001 Supplemental Figure 3. Cytosolic Z-DNA accumulation is associated with mitochondrial
1002 fragmentation.

1003 Supplemental Figure 4. IFN α does not increase mitochondrial or total cellular ROS in N/TERTs.

1004 Supplemental Figure 5. ZBP1 expression does not correlate with systemic autoantibodies or
1005 patient age.

1006 Supplemental Figure 6. mitoTEMPO rescues UVB-induced IFN expression in lupus KCs.

1007 Supplemental Figure 7. UVB leads to cytosolic shift of cGAS in N/TERTs.

1008 Supplemental Figure 8. ISGs are significantly increased after Z-DNA transfection in N/TERTs
1009 and primary KCs.

1010 Supplemental Figure 9. Overexpression of ZBP1 results in cytosolic expression.

1011 **Tables S1 to S4:**

1012 Supplemental Table 1. Demographics and characteristics of patients and controls for primary
1013 keratinocyte cell culture

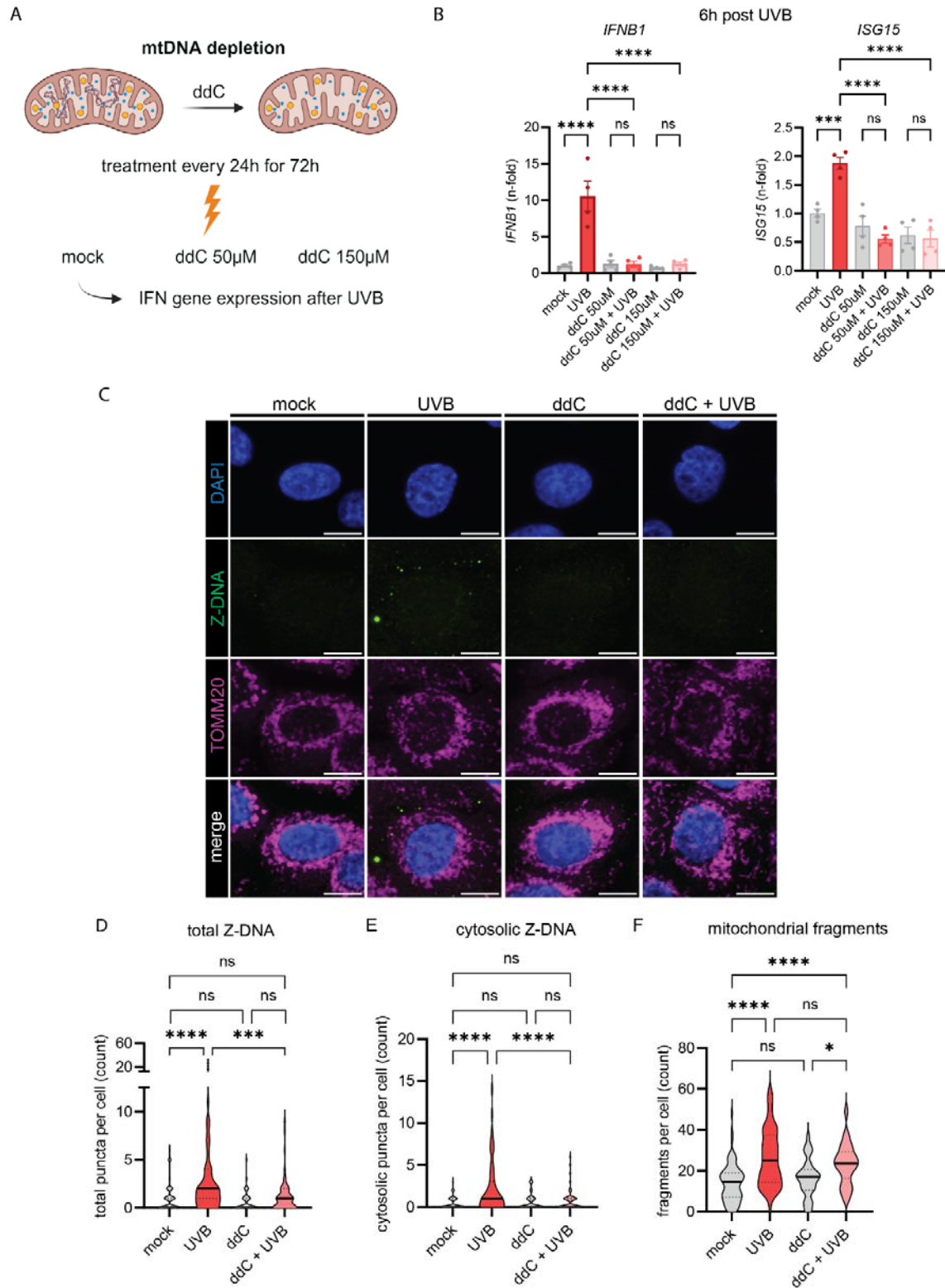
1014 Supplemental Table 2. Demographics and characteristics of lupus and dermatomyositis patients
1015 from which skin biopsies were used for tissue immunofluorescence

1016

1017 **Supplemental Data**

1018

1019 **Supplemental Figure 1**



1020

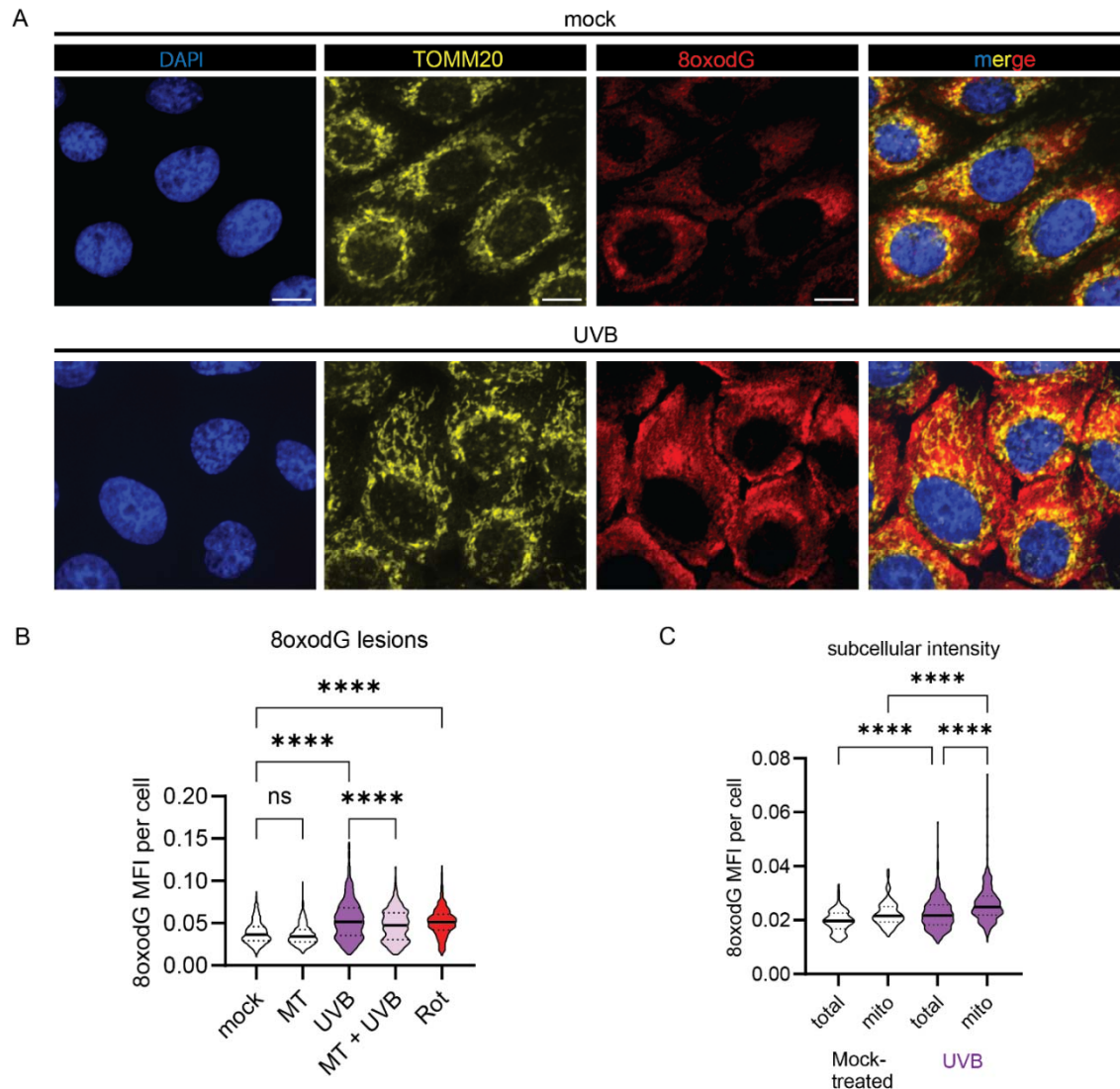
1021

1022 **Supplemental Figure 1. UVB-driven IFN responses are mtDNA dependent and UV-induced Z-DNA**
1023 **derives from mtDNA.**

1024 **A.** Experimental approach for mtDNA depletion in N/TERTs using nucleoside 2',3' dideoxycytidine (ddC).
1025 Treatment with ddC was performed for 72h. After irradiation, medium was changed to ddC-free medium
1026 until gene expression analysis. **B.** Quantitative gene expression 6h after UVB exposure. n=2 for each
1027 experiment. **C.** Representative confocal images of N/TERTs treated with +/- ddC +/- UVB 3h after UVB
1028 exposure stained for Z-DNA, TOMM20 and DAPI. Scale bar 10µm. **D.** Quantification of Z-DNA puncta
1029 and mitochondrial fragments using CellProfiler open-source software from conditions in (**C.**), n=3.
1030 Comparisons were done via ordinary one-way ANOVA followed by Sidak's multiple comparison test.
1031 Mean and SEM. *P<0.05, **P<0.01, ***P<0,001, ****P<0.0001.

1032

1033 **Supplemental Figure 2.**

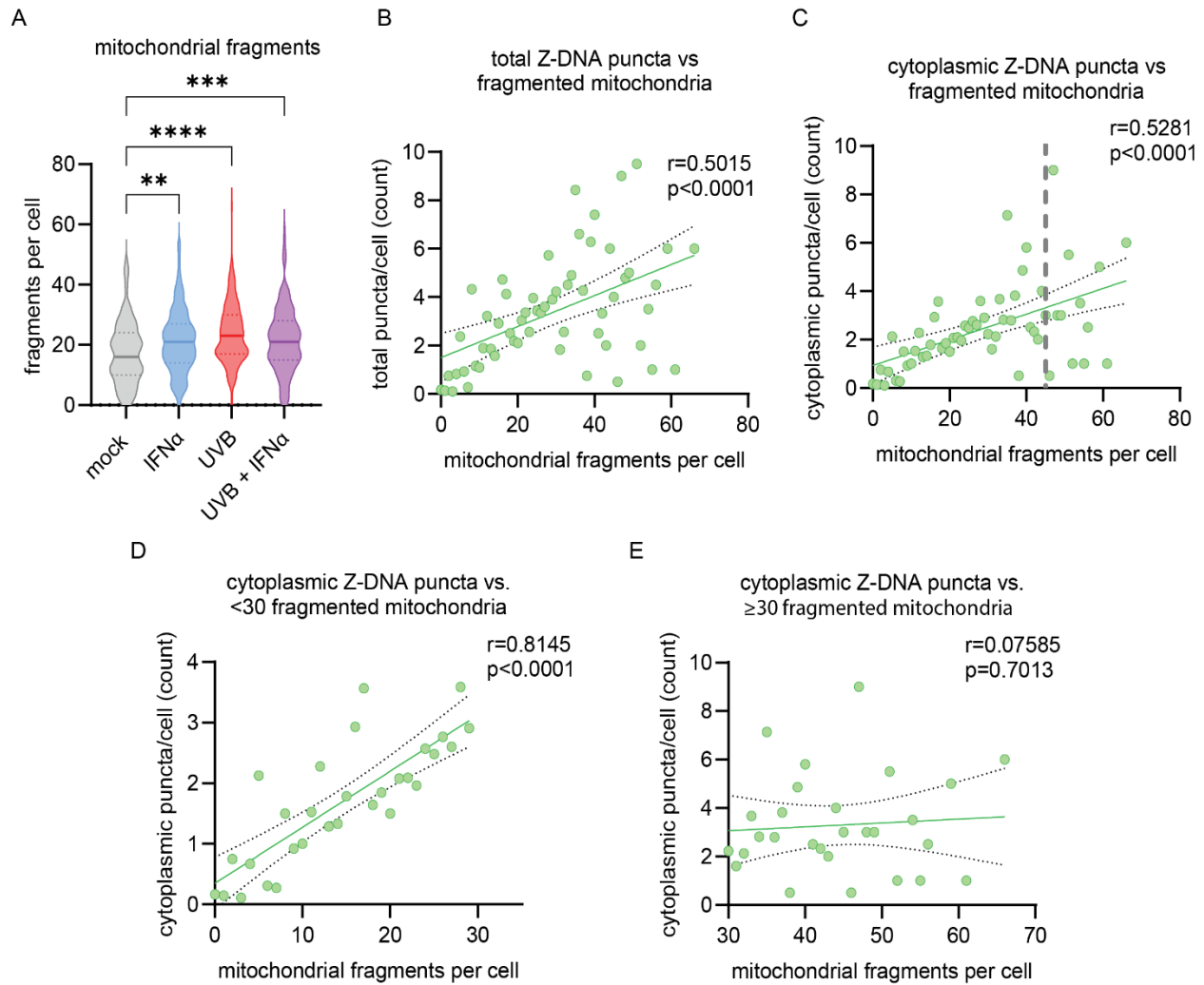


1034

1035 **Supplemental Figure 2. UVB induces oxidative DNA damage in the cytosol and mitochondrial**
1036 **compartment.**

1037 **A.** Representative confocal microscopy images of N/TERTs 3h after UVB exposure stained for TOMM20,
1038 8oxodG lesions and DAPI. Scale bar 20 μ m. **B.** Quantification of 8oxodG intensity per cell using open-
1039 source software, CellProfiler, in N/TERTs treated +/- mitoTEMPO (50 μ M), +/-UVB or Rotenone (0.5 μ M)
1040 as a positive control, n=3. **C.** Quantification of subcellular intensity of 8oxodG intensity per cell (total) or
1041 mitochondrial (mito) assessed by TOMM20⁺ merged area. Comparisons were done via ordinary one-way
1042 ANOVA followed by Sidak's multiple comparison test. Mean and SEM. *P<0.05, **P<0.01, ***P<0.001,
1043 ****P<0.0001.

1044 **Supplemental Figure 3.**



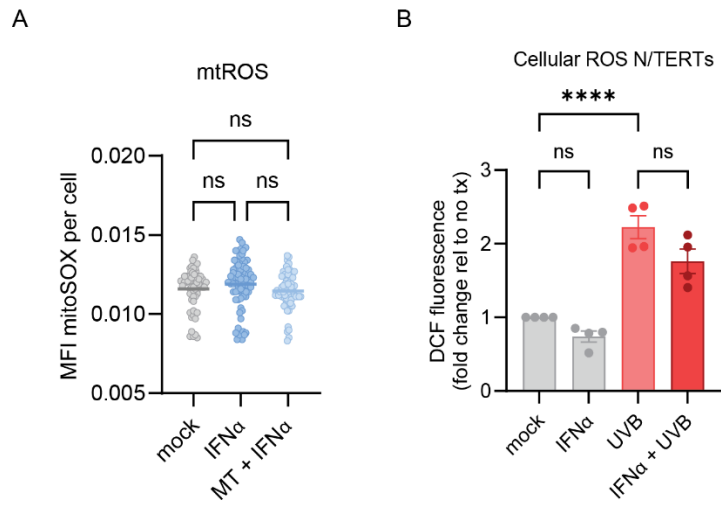
1045

1046 **Supplemental Figure 3. Cytosolic Z-DNA accumulation is associated with mitochondrial**
1047 **fragmentation.**

1048 **A.** Violin plots represent quantification of mitochondrial fragments (defined as TOMM20⁺ objects smaller
1049 than 1 μ m) in N/TERTs after 16h of IFN α treatment followed by UVB (50mJ/cm²) exposure. Comparisons
1050 were done via ordinary one-way ANOVA followed by Sidak's multiple comparison test. **P<0.01,
1051 ***P<0,001, ****P<0.0001. **B and C.** Correlation of total or cytoplasmic Z-DNA puncta and fragmented
1052 mitochondria with simple linear regression. **D and E.** Correlations of data in C divided by # of
1053 mitochondrial fragments per cell. Pearson correlation coefficient (r) and p-values for indicated correlations
1054 are shown in the upper right.

1055

1056 **Supplemental Figure 4.**



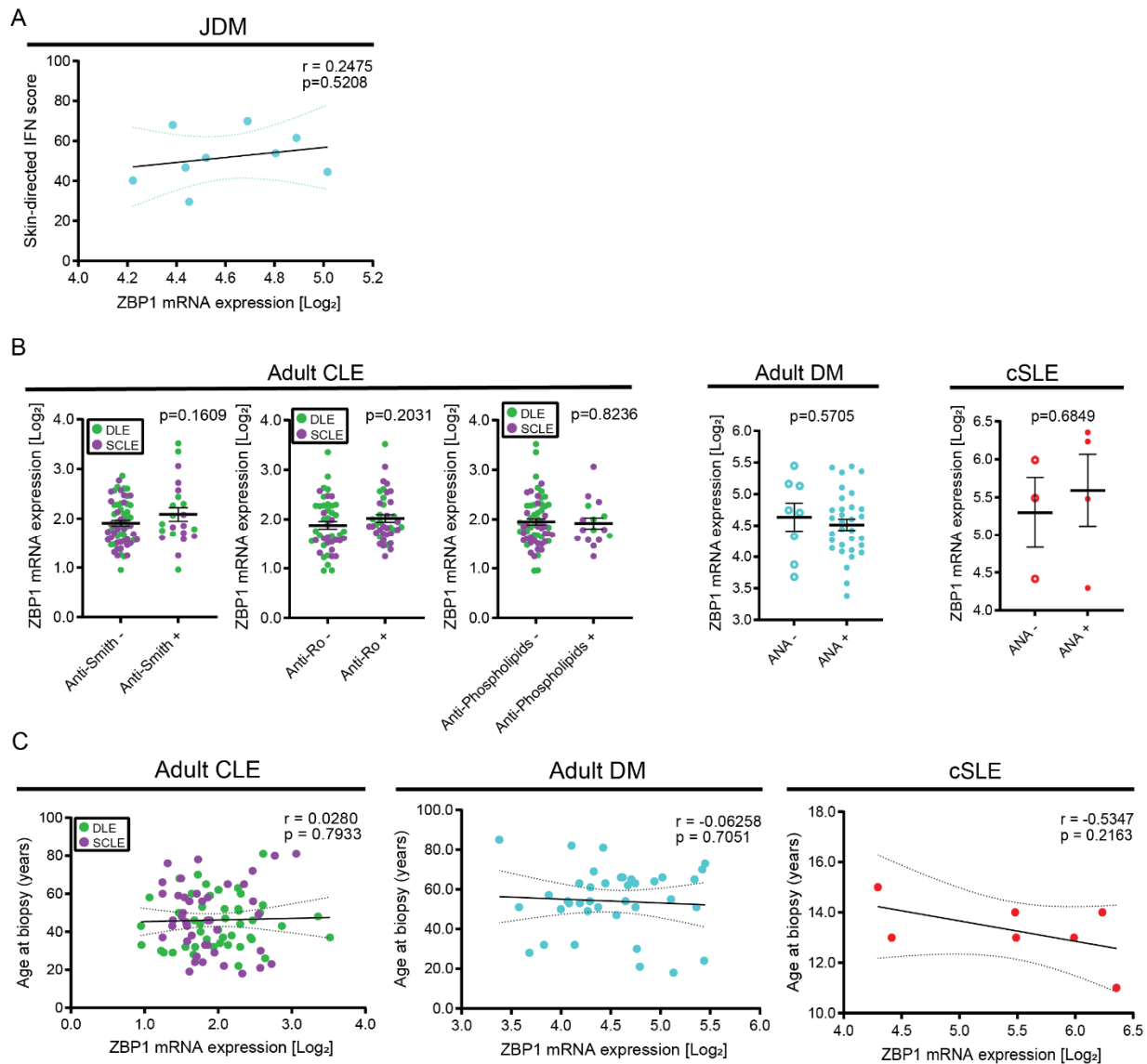
1057

1058 **Supplemental Figure 4. IFN α does not increase mitochondrial or total cellular ROS in N/TERTs.**

1059 **A.** Violin plots represent quantification of mitoSOX staining intensity per cell in N/TERTs stimulated with
1060 IFN α (1000U/ml) for 16h compared to mock. **B.** Fold change of fluorescence of
1061 Dichlorodihydrofluorescein (DFC) after treatment with IFN α for 16h +/- UVB exposure in N/TERTs 5min
1062 after UVB exposure, n=4. Comparisons were done via ordinary one-way ANOVA followed by Sidak's
1063 multiple comparison test. Mean and SEM. ****P<0.0001.

1064

1065 **Supplemental Figure 5.**



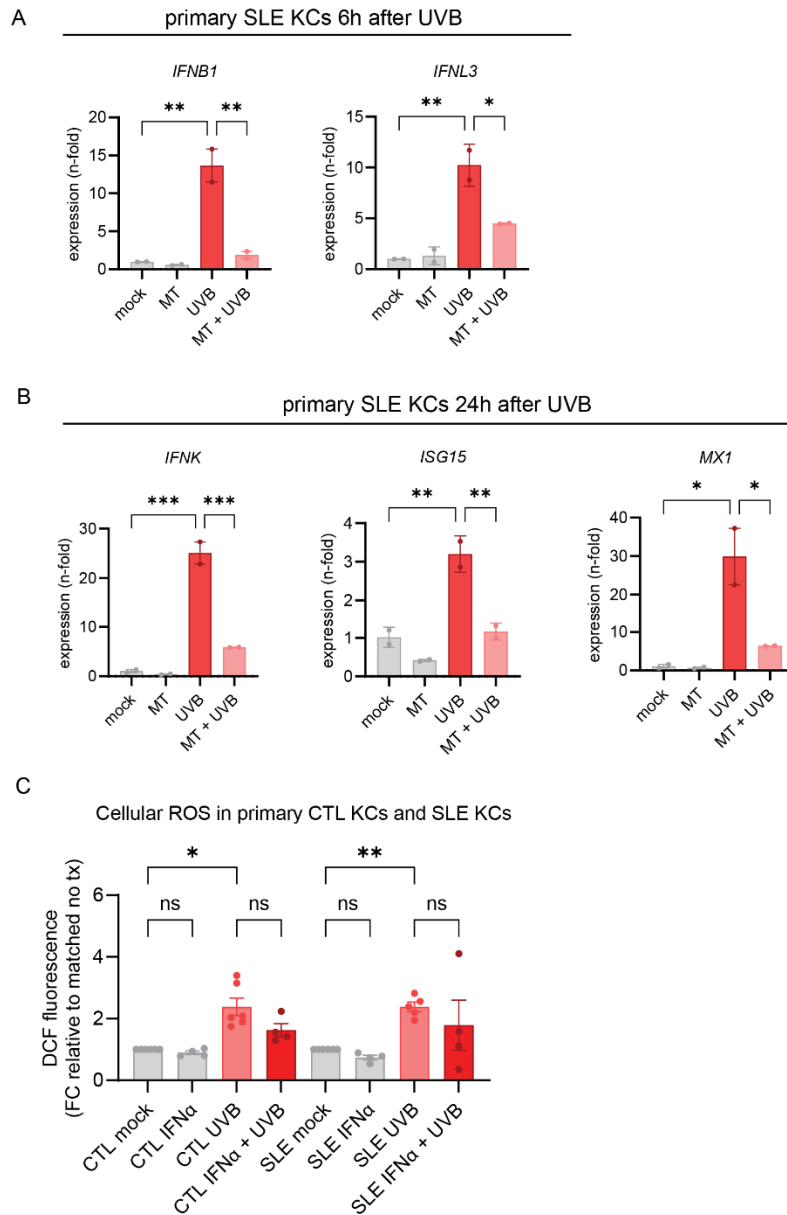
1066

1067 **Supplemental Figure 5. ZBP1 expression does not correlate with systemic autoantibodies or**
1068 **patient age.**

1069 **A.** Correlation of cutaneous *ZBP1* expression in juvenile dermatomyositis (n=9) with skin-directed IFN
1070 score showing no significant correlation. **B.** Comparison of cutaneous *ZBP1* expression with
1071 autoantibodies in adult CLE, DM and childhood onset SLE (cSLE) showing independence of *ZBP1*
1072 expression with autoantibody status. **C.** Correlation of cutaneous *ZBP1* expression with age in adult CLE,
1073 adult DM and childhood SLE (cSLE) showing no significant correlation with age.

1074

1075 **Supplemental Figure 6.**



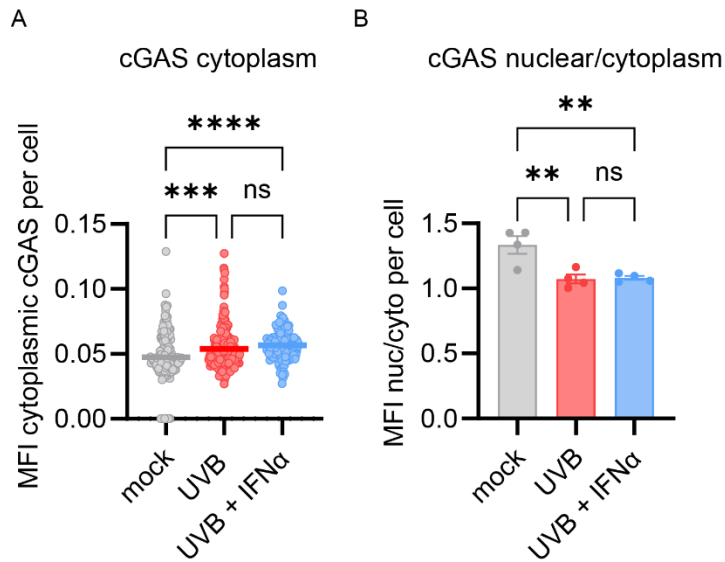
1076

1077 **Supplemental Figure 6. mitoTEMPO rescues UVB-induced IFN expression in lupus KCs.**

1078 **A.** Nonlesional SLE KCs (n=2) were treated +/- mitoTEMPO (50μM) and irradiated with UVB. Gene
 1079 expression was analyzed 6h after UVB exposure. **B.** Gene expression analysis 24h after UVB exposure
 1080 was normalized to β-Actin. n=2. Mean and SEM. **C.** Measurement of cellular ROS in primary HC KCs
 1081 (n=4) and SLE KCs (n=4) at baseline and after IFNα treatment +/- UVB exposure. Comparisons were
 1082 done via ordinary one-way ANOVA followed by Sidak's multiple comparison test. Mean and SEM.
 1083 *P<0.05, **P<0.01, ***P<0.001, ****P<0.0001.

1084

1085 **Supplemental Figure 7.**



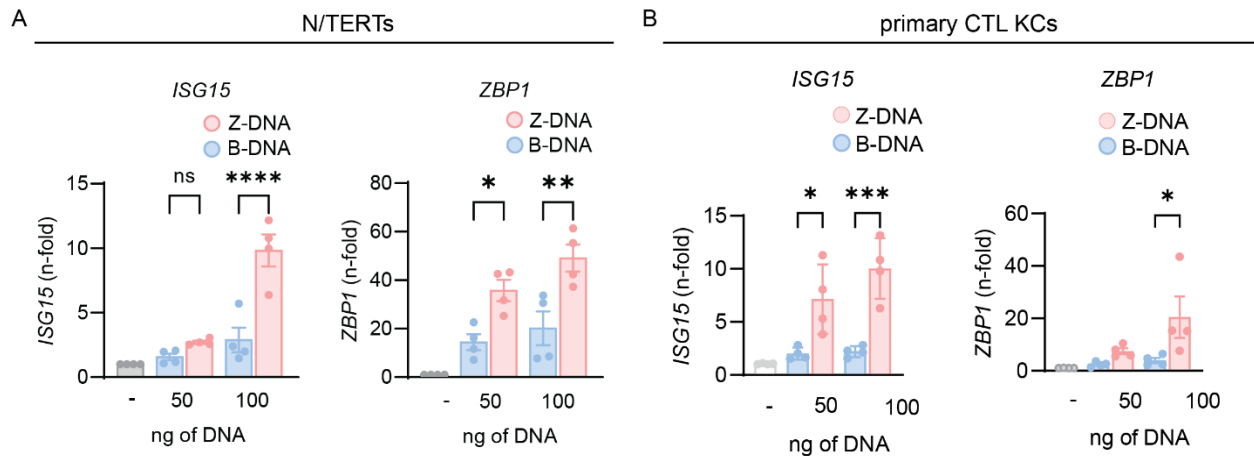
1086

1087 **Supplemental Figure 7. UVB leads to cytosolic shift of cGAS in N/TERTs.**

1088 **A.** Quantification of cytosolic mean fluorescence intensity (MFI) of cytoplasmic cGAS defined by the
1089 DAPI-negative area in N/TERTs using open-source software CellProfiler. **B.** Ratio of nuclear and
1090 cytoplasmic MFI per cell and shown is the mean ratio per cell of each experiment (n=4). Comparisons
1091 were done via ordinary one-way ANOVA followed by Sidak's multiple comparison test. Mean and SEM.
1092 **P<0.01, ***P<0,001, ****P<0.0001.

1093

1094 **Supplemental Figure 8.**



1095

1096 **Supplemental Figure 8. ISG15 and ZBP1 are significantly increased after Z-DNA transfection vs.**

1097 **B-DNA in N/TERTs and primary KCs.**

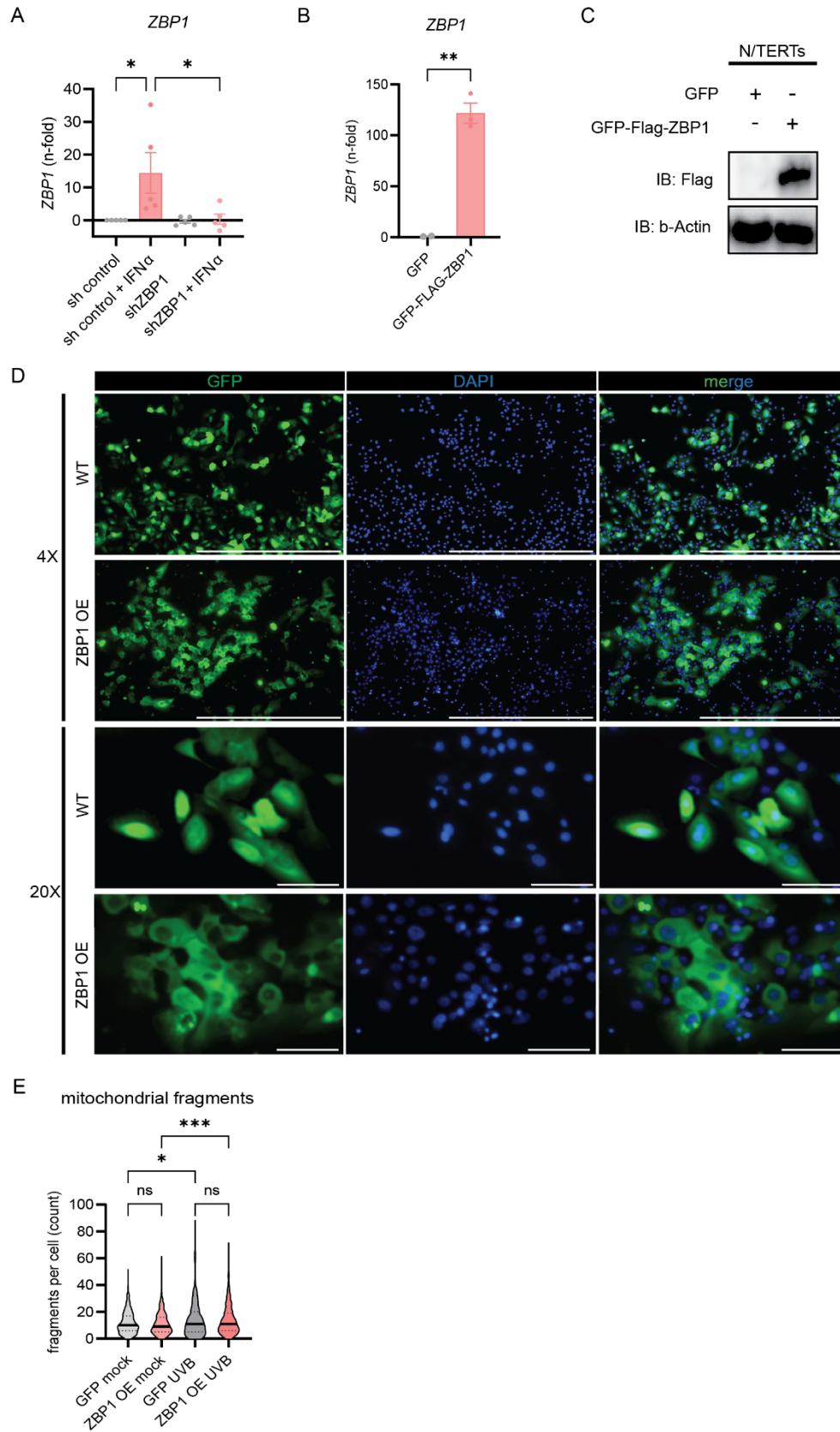
1098 **A.** Gene expression at 24h of indicated genes from N/TERTs (n=4) and primary HC KCs (n=4) treated
1099 transfected with Z-DNA or B-DNA. Comparisons were done via ordinary one-way ANOVA followed by
1100 Sidak's multiple comparison test. Mean and SEM. **P<0.01, ***P<0.001, ****P<0.0001.

1101

1102

1103

1104 **Supplemental Figure 9.**



1106 **Supplemental Figure 9. Overexpression of ZBP1 results in cytosolic expression.**

1107 **A.** Confirmation of shRNA knockdown by qPCR compared to shcontrol after IFN α stimulation (1000U/ml)
1108 for 16h, n=5. **B.** Quantitative gene expression of ZBP1 overexpressors compared to GFP alone, n=3.
1109 **C.** Immunoblot against FLAG confirming FLAG-tag of ZBP1 overexpressor cells. **D.** Representative
1110 immunofluorescence images show efficient transfection of both GFP (first line) alone and GFP-ZBP1
1111 (second line) in 4X magnification, scale bar=1000 μ m. Detailed images reveal pancellular tag of GFP (third
1112 line) and cytosolic overexpression of ZBP1 (fourth line). 20X, scale bar=1000 μ m. 4X, scale bar=100 μ m.
1113 **E.** Quantification of mitochondrial fragments (TOMM20⁺ objects <1 μ m² with circularity >0.6) in GFP-tag
1114 N/TERTs and ZBP1 OE N/TERTs at baseline and after UVB exposure using CellProfiler software.
1115 Comparisons were done via ordinary one-way ANOVA followed by Sidak's multiple comparison test or t-
1116 test. *P<0.05, **P<0.01, ***P<0,001, ****P<0.0001.

1117

1118 **Supplemental Table 1. Demographics and characteristics of patients and controls for primary**
 1119 **keratinocyte cell culture**

	HC (N=8)	SLE (N=8)
Median age in years (IQR)	44 (31,52)	44 (41,52)
Female sex - n (%)	4 (50%)	6 (75%)
Cutaneous lupus – n (%)	-	5 (62%)
Median SLEDAI-2k (IQR)	-	2 (0,4)
Cutaneous lupus subtype – n (%)		
ACLE	-	1 (12%)
SCLE	-	1 (12%)
DLE	-	3 (38%)
CLASI activity (IQR)		2 (0,3)
SLE treatment – n (%)		
Hydroxychloroquine	-	5 (62%)
Glucocorticoid	-	3 (38%)
Immunosuppressant	-	7 (88%)
Autoantibodies – n positive (%)	-	
ANA	-	8 (100%)
Anti-Ro/SSA	-	5 (62%)
Anti-dsDNA	-	4 (50%)
Anti-Sm/RNP	-	4 (50%)
Site of non-lesional biopsy - n (%)		
Buttock/hip	8 (100%)	7 (88%)
Arm	0	1 (12%)
HC: healthy controls; SLE: systemic lupus erythematosus; IQR: interquartile range; n: number; SLEDAI: Systemic Lupus Erythematosus Disease Activity; ACLE: acute cutaneous lupus; DLE: discoid lupus erythematosus; SCLE: subacute cutaneous lupus erythematosus; CLASI: Cutaneous Lupus Erythematosus Disease Area and Severity Index; ANA: antinuclear antibody		

1120
 1121

1122 **Supplemental Table 2. Demographics and characteristics of lupus and dermatomyositis**
 1123 **patients from which skin biopsies were used for tissue immunofluorescence**

	CLE/SLE (N=13)		DM (N=6)	
Median age in years (IQR)	46 (41,51)		54 (35,61)	
Female sex - n (%)	11 (85%)		5 (83%)	
	Clinical manifestations CLE/SLE		Clinical manifestations DM	
	Cutaneous lupus only – n (%)	4 (31%)	Skin involvement	6 (100%)
	DLE	8 (62%)	Muscle involvement	4 (67%)
	SCLE	5 (38%)		
	Median CLASI activity (IQR)	4 (2,8)		
	Median SLEDAI-2k (IQR)	4 (2,8)		
Autoantibodies – n positive (%)				
ANA	12 (92%)		5 (83%)	
	Anti-Ro/SSA	6 (46%)	Anti-Mi-2	1 (17%)
	Anti-dsDNA	4 (31%)	Anti-TIF-1γ	1 (17%)
	Anti-Sm/RNP	3 (23%)	Anti-PL7	1 (17%)
Treatment – n (%)				
Hydroxychloroquine	12 (92%)		2 (33%)	
Glucocorticoid	6 (46%)		1 (17%)	
Immunosuppressant	5 (38%)		3 (50%)	
SLE: systemic lupus erythematosus; CLE: cutaneous lupus erythematosus; DM: dermatomyositis; IQR: interquartile range; n: number; DLE: discoid lupus erythematosus; SCLE: subacute cutaneous lupus erythematosus; CLASI: Cutaneous Lupus Erythematosus Disease Area and Severity Index; SLEDAI: Systemic Lupus Erythematosus Disease Activity; ANA: antinuclear antibody				